CHALMERS
UNIVERSITY OF TECHNOLOGY

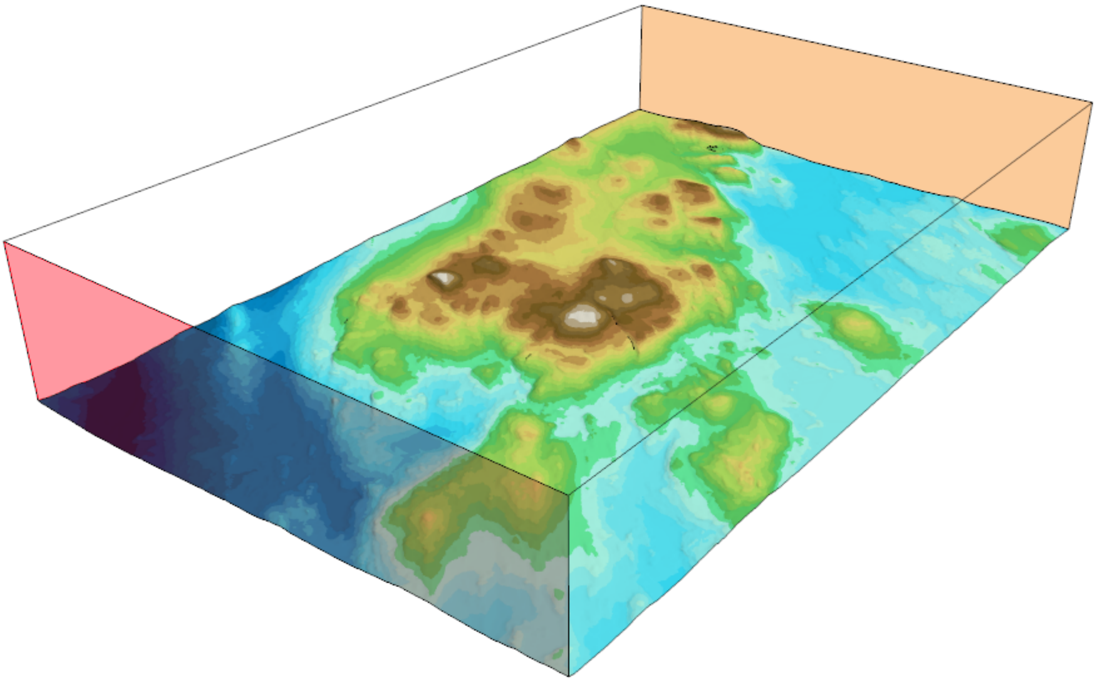

CFD Modeling of a Neutral Atmospheric Boundary Layer over Complex Terrain

Applied Mechanics

KÁRI BREKASON

Department of Mechanics and Maritime Sciences
CHALMERS UNIVERSITY OF TECHNOLOGY
Gothenburg, Sweden 2018

Master's thesis 2018:24

CFD Modeling of a Neutral Atmospheric Boundary Layer over Complex Terrain

KÁRI BREKASON

Department of Mechanics and Maritime Sciences
Division of Fluid Dynamics
Chalmers University of Technology
Gothenburg, Sweden 2018

CFD Modeling of a Neutral Atmospheric Boundary Layer over Complex Terrain
Kári Brekason

Supervisor: Hamidreza Abedi, Division of Fluid Dynamics
Examiner: Lars Davidson, Division of Fluid Dynamics

Master's Thesis 2018:24
Department of Mechanics and Maritime Sciences
Division of Fluid Dynamics
Chalmers University of Technology
SE-412 96 Gothenburg
Telephone +46 31 772 1000

Cover: Computational domain generated through the use of topography data of the terrain surrounding Rödbergskullen wind farm.

Typeset in LaTeX
Gothenburg, Sweden 2018

CFD Modeling of a Neutral Atmospheric Boundary Layer over Complex Terrain
Kári Brekason
Department of Mechanics and Maritime Sciences
Chalmers University of Technology

Abstract

As wind energy production continues to grow the most optimal areas for wind energy generation have quickly been utilised. As wind farms are more frequently placed in less optimal areas, the need for methods to accurately site these areas becomes paramount. One such method is to use *Computational Fluid Dynamics* (CFD) models of the atmospheric boundary layer to predict the flow structures above sites which are located in complex terrain. This study investigates the use of *Detached Eddy Simulations* (DES) as well as *Large Eddy Simulations* (LES) to quantify the effects of flow over complex terrain. The simulated wind fields are used in combination with an aero-elastic solver to assess the dynamic response of a wind turbine. It is found that the protective properties of boundary layers in DES is such that it makes it inconvenient for generating a fluctuating wind field since it dampens out fluctuations in altitudes occupied by wind turbines. LES is found to replicate well the predicted turbulence as well as time-averaged velocity profiles even though no rough wall treatment is used. However, discrepancies are found when investigating the Reynolds stresses that result from a combination of a too short sampling time and symmetric boundary conditions. Albeit these discrepancies the wind fields generated through LES are used with an aero-elastic solver to simulate the dynamic response of a "NREL 5-MW Baseline Wind Turbine". The results show that the wind turbine located in complex terrain is subject to more fatigue than if it is placed on flat terrain. The identified load cycles are however relatively few and so the simulation time should be increased to get a better statistical representation. Due to the discrepancies resulting from symmetric boundaries and short sampling time the effect of complex terrain is not quantified with any certainty. However, LES in the absence of complex wall functions is proven useful as a tool to assess wind fields over complex terrain. Further investigation is necessary where it is recommended that boundaries be assigned differently and longer sampling times be used.

Keywords: Wind turbine, Complex terrain, Atmospheric Boundary Layer, Large eddy simulation, Detached eddy simulation.

Acknowledgements

First of all I would like to express my deepest gratitude to Hamidreza Abedi for all the productive discussions we have had over the course of this project and for all the good help he has provided. I would like to thank my friend and fellow student Madhavan Vasudevan for valuable discussions and moral support. I am also grateful of the discussions and input provided by Elías Mikael Vagn Siggeirsson and other members of the Division of Fluid Dynamics. I would then like to thank all my fellow students who have helped me in the years leading up to this project. Finally I would like to thank Helga for all the love and support.

Kári Brekason, Gothenburg, June 2018

Nomenclature

Abbreviations

CFD Computational Fluid Dynamics

LES Large Eddy Simulation

DES Detached Eddy Simulation

RANS Reynolds Averaged Navier-Stokes

a.g.l Above Ground Level

a.s.l Above Sea Level

ABL Atmospheric Boundary Layer

BEM Blade Element Momentum method

CAE Computer Aided Engineering

FAST Fatigue, Aerodynamics, Structures and Turbulence

ISA International Standard Atmosphere

Met mast Meteorological measurement mast

SGS Subgrid Scale

Turbulence Modelling

Δ Filter width

δ_{ij} Dirac delta operator

κ von Karman constant

$\langle u \rangle$ Mean velocity in streamwise direction

μ Dynamic viscosity

ν Kinematic viscosity

ν_t Turbulent viscosity

ν_{SGS} Subgrid scale viscosity

$\overline{u}$ Filtered velocity in streamwise direction

ρ	Density
σ_ε	k-ε model constant
σ_k	Turbulent Prandtl number, k-ε model constant
τ_{ij}	Subgrid scale stresses
ε	Turbulent dissipation rate
C_μ	k-ε model constant
C_S	Smagorinsky model constant
$C_{\varepsilon 2}$	k-ε model constant
$C_{\varepsilon 1}$	k-ε model constant
f_i	External force
I	Turbulent intensity
k	Turbulent kinetic energy
P	Pressure
p	Hydrodynamic pressure
S	Strain rate
t	Time
u	Velocity in streamwise direction
u'	Turbulent fluctuation in streamwise direction
u^+_{RH}	Roughness height dimensionless velocity
y	Wall distance
y_0	Roughness length

Blade Element Theory

β	Corrected flow angle
λ_r	Local tip speed ratio, $\lambda_r = \frac{\Omega r}{V}$
Ω	Rotational speed
ρ	Density
σ'	Local solidity factor, $\sigma' = \frac{Bc}{2\pi r}$
a	Axial induction factor
a'	Tangential induction factor
A_{el}	Area of single blade element

B	Number of blades
c	Blade element chord length
C_D	Drag coefficient
C_L	Lift coefficient
$F_{\theta,el}$	Elemental force perpendicular to flow
$F_{x,el}$	Elemental force parallel to flow
Q	Tip loss correction factor, $(0 < Q < 1)$
r	Radial distance to turbine hub
V	Relative flow velocity
W	Corrected total velocity

Contents

List of Figures

List of Tables

1

Introduction

In recent years wind energy as a percentage of total energy consumed in Sweden has increased substantially. During the ten year span from 2006 to 2016 this percentage has gone from 1% to 15% [7]. As wind farms have quickly occupied the most optimal locations for wind energy generation there is an increasing need to occupy less optimal areas. However, poorly sited wind farms may yield costly energy production due to high maintenance and/or inefficient energy production. In order to assess the quality of potential sites, on-site measurements are used but they can only provide local values which are of limited use when compared to how large wind patterns are. This raises a demand for accurate computer simulations which can predict well the structures and patterns in atmospheric wind flows.

Simulation techniques for wind turbine responses are accurate and computationally inexpensive. Their accuracy is however completely dictated by an accurate description of the incoming wind pattern. In simple cases the wind patterns may be replicated to a high degree of accuracy but as the terrain increases in complexity so do the wind patterns. With modern computational power the time-average of these complicated patterns can be predicted with fair accuracy using CFD models. Because of the turbulent (seemingly random) behaviour of the wind patterns these time-averaged results prove insufficient for use when predicting fatigue loads on a turbine blade or other components of a wind turbine. This is where transient model simulations may excel, at the added cost of computational power.

This study will focus on generating a transient CFD model of atmospheric boundary layer flow to study the effects of complex terrain on the dynamic response of a wind turbine.

1.1 Simulation techniques for wind turbines

Modern structural simulations and CAE methods make the detailed analysis of structures possible. Structures can be inspected for their static and dynamic behaviour with relatively good accuracy at a rather low computational cost. The previous statement does however assume that the applied forces in the structural models are correct. This is where structural analysis becomes difficult.

Modern models of wind turbines utilise a combination of a blade element approach together with the conservation of momentum to calculate the forces that arise on turbine blades as they are exposed to the wind. Because of the turbulent nature of wind fields these forces will vary with time. From a structural point of view this is not a problem as sufficiently small time steps combined with implicit time discretisations may resolve the dynamic responses of the turbine blades. Even the control signals for blade pitch can be emulated using these models. The underlying fact however is that all these depend on the accurate description of the time dependent wind field.

1.2 Literature survey

The flow of air past simple shapes like wedges or single hills has been the focus of many CFD studies. The main problem that researchers face is that different CFD models produce different results and while one model might resolve one particular flow well compared to actual measurements, that same model might prove infeasible for other types of flows. An example of such a study is the modelling of flow over the Askervein Hill. The Askervein Hill, standing 116 m tall on an island in Scotland, is surrouded by relatively flat lands and was the focus of several studies in 1982 and 1983 [15][16][17]. Using field measurements from the Askervein Hill for comparison, fairly accurate results have been gathered using k-ε models to simulate the mean flow fields [11]. These simulations were conducted with neutral atmospheric conditions using wall functions to account for surface roughness and the results show a good agreement with respect to wind speed profiles.

The quality of mean flow simulations over complex terrain are dictated to a high degree of chosen inlet conditions. Therefore inlet conditions of simulations should be chosen with great care in order to eliminate unrealistic results. For a neutrally stratified boundary layer these conditions have been derived analytically using the assumption of constant shear stress which makes the modelling of a neutral atmospheric boundary layer a practical choice. Another important concept is that the inlet must be sufficiently far away from the area of interest or in other words that the upwind fetch from the region of interest be sufficient. This is because the flow field must be allowed to develop from inlet conditions to form any local structures [4].

As for transient flow fields *Large Eddy Simulations* (LES) are preferable for modelling purposes. However it imposes the need for an extremely fine mesh resolution in the near wall regions. Since atmospheric domains are generally in the size range of kilometres this renders it almost unusable. However LES can be combined with *Reynolds Averaged Navier-Stokes* (RANS) to form a hybrid model (hybrid LES-RANS). Such a hybrid model has been shown to predict well the flow structures over the Askervein Hill [2]. The model in question combines the two models by choosing a turbulent length scale from the minimum of the RANS length scale or local grid size the net effect of which treats the outer layer as LES while the lowest 10 m or so of the domain is treated in a RANS formulation. Since the boundary of LES and RANS will exhibit a large jump in velocity, a backscatter model is used to provide a bridge using stochastic variables to generate turbulence. A later study using the same hybrid model neglects this backscatter stating that it is negligible for flows over complex terrain [3]. Both these studies were done using an in-house code and currently commercial codes such as *StarCCM+* do not provide such hybrid LES-RANS models. *StarCCM+* does however currently provide *Detached Eddy Simulation* (DES) models which are similar albeit one main difference. The difference is that DES applies RANS to boundary layers as a whole while hybrid models only attempt to model the inner most part of boundary layers [6].

1.3 Röbergskullen wind farm

The Rödbergskullen wind farm is situated on a hill (540 m a.s.l) roughly 100 km north of Karlstad, Sweden. It is comprised of eight Vestas V90 horizontal axis wind turbines, each with a capacity of 2 MW. These wind turbines have a hub height of 80 m while the rotor diameter is 90 m resulting in a total height of 125 m. Since the wind farm is located in an area with complex terrain it makes for an ideal location on which to base this study. Measurements of wind speeds have been collected over a period prior to this project with which simulation results may be compared. Also these local measurements may be useful in determining a suitable wind speed, direction and levels of turbulence.

Figure 1.1: A perspective view of the Rödbergskullen wind farm, from [18].

During the wind farms operation it has become apparent that the occurrence of mechanical failures is higher than expected especially for some turbines. These mechanical failures occur in the gearboxes but there is visual evidence that the gearbox wants to break free from where it is fastened. These wind turbines are equipped with control mechanisms to keep torque values under set limits so high wind speeds should not be problematic. However if turbulent fluctuations are large it might be possible for a control mechanism to lag behind fluctuations resulting in high loads. These high loads might not exceed static maximum values but in terms of fatigue these high loads might result in a shorter than expected lifetime of components. It shall be said that the proposed cause is not the only possible explanation behind these failures but in the scope of this study it is interesting how turbulent structures caused by complex terrain relate to loads applied to the turbines.

1.4 Objectives and limitations

The main objective of this project is to study the effect of complex terrain on the turbulent nature of a flow field and the dynamic response of a wind turbine. The method used to achieve this is the generation of transient flow fields over both flat and complex terrains using identical boundary conditions. Apart from only comparing these two flow fields, the flow fields are used to evaluate the dynamic response of a wind turbine using an aero-elastic solver. The different responses can then also be compared.

The main objectives and limitations of this study have been summarised in the following list:

- Utilise CFD models known to predict well the time-averaged behaviour of a neutral atmospheric boundary layer to assess the shape of flow structures over Rödbergskullen.

- Using the time-averaged results as reference, establish a CFD model to predict the transient behaviour of the neutral atmospheric boundary layer.

- Study the dynamic response of a wind turbine using the transient generated wind fields combined with aero-elastic solver.

- Quantify the main differences found between the flow over flat and complex terrains in terms of the flow and the response of the wind turbine.

- The quality of the transient flows simulated are only evaluated against mean flows generated with CFD as opposed to actual measurements.

- The CFD study is limited to the use of *Star-CCM+* and the models it provides.

- The CFD study is limited by the amount of computational resources available.

2

Theory

2.1 Neutral Atmospheric Boundary Layer

The *Atmospheric Boundary Layer* (ABL) is the lowest part of the atmosphere. At the very top of the ABL the wind speed equals that of the geostrophic wind but at ground level surface (grass, trees, buildings etc.) reduces the wind speed to zero with a logarithmic velocity profile. In the lowest part of the ABL turbulent fluxes can be considered constant and Coriolis forces of low importance. This lowest part of the ABL is called the surface layer. The total height of the ABL may vary depending on thermal stratification and other factors but it is in the range of kilometers [2].

2.1.1 Atmospheric stability

The height of the ABL can vary significantly but it is governed to a large extent to its thermal stratification. During daytime the sun will heat up the ground through radiation which in turn will create large thermal flow structures which stretch the ABL height. The temperature decreases with altitude and stratification is said to be unstable as turbulence is amplified with increased altitude. During night time the situation is reversed. Temperature increases with altitude and turbulence is damped with altitude. The stratification is then said to be stable. A condition in between stable and unstable is the neutral stratification where temperature is constant with altitude causing neither an increase or decrease in turbulence with altitude. This is the Neutral Atmospheric Boundary Layer [2].

2.1.2 Effects of geographical height variations

It is documented that variations in the height of landscape affects local wind speed. This change in velocity has been shown to exist through measurements made over hills such as the Askervein Hill mentioned in section 1.2. The changes are such that at the top of hills and mountains the wind speed is relatively higher than around it.

This relative speed-up can be as high as 80% compared to values upstream of the hill or mountain. Shown in Figure 2.1 is the speed-up of wind over a hill depicted graphically.

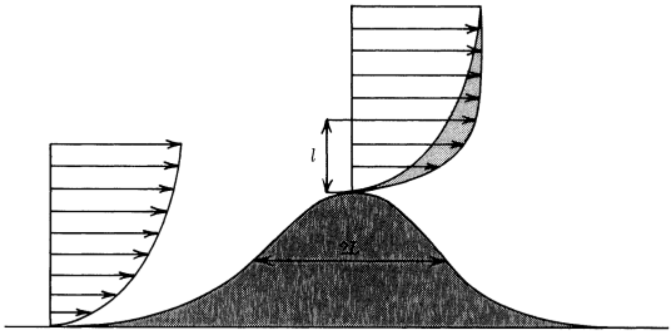

Figure 2.1: A graphic depiction of relative speed-up of wind over a hill (figure from [19]).

2.2 Computational Fluid Dynamics

Computational Fluid Dynamics (CFD) is the use of numerical methods to obtain approximate solutions of problems of fluid dynamics or heat transfer [21]. To solve such problems numerically, one first needs a mathematical description of the system. This description comes from the equations of conservation of mass (continuity), conservation of momentum (Newton's second law of motion, for fluids often referred to as the Navier-Stokes equation) and conservation of energy (first law of thermodynamics). For a problem where energy transfer is negligible or non existent the conservation of energy can be left out.

For atmospheric flows the velocities are relatively low allowing it to be treated as incompressible flow. When neutrally stratified, energy transfer can also be neglected. This allows the treatment of temperature and viscosity as global constants. This treatment is used throughout this study and all equations presented hereafter account for this.

2.2.1 Turbulence models

Calculating the Reynolds number of atmospheric flow using a characteristic velocity of 10 m/s, length scale of 1000 m and dynamic viscosity of 1.8e-5 Pa s yields:

$$Re_L = \frac{U\ell}{\nu} = \frac{10 \cdot 1000}{1.8\text{e-}5} = 5.6\text{e}8 \tag{2.1}$$

When comparing this to flow over a flat plate this Reynolds number is well above the turbulent reference value of 5e5. This means that when dealing with flow of an ABL the flow is turbulent. The flow still adheres to the Navier-Stokes equation but velocity components in turbulent flow do not reach a steady value but rather fluctuate continuously. This presents an additional challenge for the CFD approach because the turbulent nature is computationally expensive to resolve. However, the need for computational power is reduced by using turbulence models. Different turbulence models exist but the ones utilised for this study are briefly explored in sections 2.2.1.1, 2.2.1.2 and 2.2.1.3.

2.2.1.1 Reynolds Averaged Navier-Stokes with two equation model

As mentioned previously, turbulent flow quantities do not reach a steady state with respect to time which presents a problem when solving the flow field numerically. To work around this the Navier-Stokes and continuity equations may be solved as time-averages. This is approached by breaking up the instantaneous velocity as a sum of a mean and a fluctuating part. Assuming a steady state has been reached, conservation of mass and momentum can then be expressed as [6]:

$$\frac{\partial \langle v_i \rangle}{\partial x_i} = 0 \tag{2.2}$$

$$\rho \frac{\partial \langle v_i \rangle \langle v_j \rangle}{\partial x_j} = -\frac{\partial \langle p \rangle}{\partial x_i} + \mu \frac{\partial^2 \langle v_i \rangle}{\partial x_j \partial x_j} - \rho \frac{\partial \langle v_i' v_j' \rangle}{\partial x_j} \tag{2.3}$$

This is commonly known as *Reynolds Averaged Navier-Stokes* (RANS). The brackets ($\langle \cdot \rangle$) denote a time-averaged quantity. When expressing conservational laws using this terminology it in turn presents a new problem because of the need to express a time-average of a multiplied quantity of fluctuations. This term is referred to as the Reynolds stress and is the last term in equation 2.3. In RANS this term is modelled. There are numerous models that exist but the model used in this study is the k-ε two equation model.

An underlying assumption of the k-ε model is the *Bossinesq assumption*. It formulates the Reynolds stress as [6]:

$$\langle v_i' v_j' \rangle = -\nu_t \left(\frac{\partial \langle v_i \rangle}{\partial x_j} + \frac{\partial \langle v_j \rangle}{\partial x_i} \right) + \frac{2}{3} \delta_{ij} k \tag{2.4}$$

Where ν_t is defined as:

$$\nu_t = C_\mu \frac{k^2}{\varepsilon} \tag{2.5}$$

The governing equations in the k-ε model is then the conservation of mass and momentum along with the transport equations for turbulent kinetic energy (k) and turbulent dissipation (ε). The transport equations for k and ε are given by equations 2.6 and 2.7 [6]:

$$\frac{\partial k}{\partial t} + \langle v_j \rangle \frac{\partial k}{\partial x_j} = \nu_t \left(\frac{\partial \langle v_i \rangle}{\partial x_j} + \frac{\partial \langle v_j \rangle}{\partial x_i} \right) \frac{\partial \langle v_i \rangle}{\partial x_j} - \varepsilon + \frac{\partial}{\partial x_j} \left[\left(\nu + \frac{\nu_t}{\sigma_k} \right) \frac{\partial k}{\partial x_j} \right] \tag{2.6}$$

$$\frac{\partial \varepsilon}{\partial t} + \langle v_j \rangle \frac{\partial \varepsilon}{\partial x_j} = \frac{\varepsilon}{k} C_{\varepsilon 1} \nu_t \left(\frac{\partial \langle v_i \rangle}{\partial x_j} + \frac{\partial \langle v_j \rangle}{\partial x_i} \right) \frac{\partial \langle v_i \rangle}{\partial x_j} - C_{\varepsilon 2} \frac{\varepsilon^2}{k} + \frac{\partial}{\partial x_j} \left[\left(\nu + \frac{\nu_t}{\sigma_\varepsilon} \right) \frac{\partial \varepsilon}{\partial x_j} \right] \tag{2.7}$$

Equations 2.6 and 2.7 are both written in terms of neglecting gravity and hence buoyant terms. C_μ, $C_{\varepsilon 1}$, $C_{\varepsilon 2}$, σ_k, σ_ε are all model constants. The k-ε model has been used to model atmospheric flow with good results and so it will serve as a good reference model when studying qualities of transient models. It is computationally inexpensive as it allows for a relatively coarse near wall resolution of the mesh.

2.2.1.2 Large Eddy Simulations

Rather than averaging over time only, *Large Eddy Simulations* (LES) makes use of an averaged quantity in time and space. The terminology of filtering is introduced where filtering refers to the time and space averaging. Conservation of mass and momentum can then be expressed as filtered quantities [6]:

$$\frac{\partial \overline{v}_i}{\partial x_i} = 0 \tag{2.8}$$

$$\rho \frac{\partial \overline{v}_i}{\partial t} + \rho \frac{\partial \overline{v}_i \overline{v}_j}{\partial x_j} = -\frac{\partial \overline{p}}{\partial x_i} + \mu \frac{\partial^2 \overline{v}_i}{\partial x_j \partial x_j} - \rho \frac{\partial \tau_{ij}}{\partial x_j} \tag{2.9}$$

The overbar ($\bar{\cdot}$) denotes a filtered quantity. The last term in equation 2.9, although it looks almost identical to the Reynolds stresses in equation 2.3, refers only to the subgrid stress. The main idea with this is that the large scales (grid scales) be resolved while the effect of small scales (subgrid scales) be modelled. This means that compared to RANS only a fraction of the turbulent quantities are modelled. How big the fraction of turbulent scales are modelled depends on how fine the filter/grid is. Because only part of the turbulence is modelled, LES is computationally more expensive than RANS. This also means that it is superior to RANS when the interests lie in the representation of a transient flow field which is the aim of this study.

There are many version of LES models but the one used for this project is the zero-equation with Smagorinsky model. Just like the k-ε model it utilizes the *Bossinesq assumption* although the expression for the turbulent viscosity is now only derived for the subgrid scales (SGS) [6]:

$$\nu_{SGS} = (C_S \Delta)^2 |\overline{S}| \tag{2.10}$$

Where C_S is a constant, Δ is the local filter width and $\overline{S}$ is the local strain rate. The unresolved stresses then become:

$$\tau_{ij} - \frac{1}{3}\delta_{ij}\tau_{kk} = -2\ \nu_{SGS}\overline{S}_{ij} \tag{2.11}$$

2.2.1.3 Detached Eddy Simulations

Due to the small scales present in boundary layers the LES formulation described in Section 2.2.1.2 requires that the near wall layers have a very fine mesh resulting in heavy computational costs. It is also limited in the availability of certain wall models which are based on time-averaged quantities often used for RANS. One way to circumvent these problems is to treat the outer layers in LES mode while retaining RANS formulation in the boundary layers near the walls. This is the idea behind Detached Eddy Simulations (DES). There are many different DES models but the one used for this study is based on combining LES with a SST-k-ω RANS model which is available in *Star-CCM+*. Detailed descriptions of the model are found in [12] but to describe it in short the model replaces the specific dissipation rate (ω) in the transport equation for k with an altered dissipation rate $\tilde{\omega}$:

$$\tilde{\omega} = \omega\phi \tag{2.12}$$

Where ϕ is taken to be:

$$\phi = \max\left(\frac{\sqrt{k}}{\beta^{*}\omega}\frac{F}{C_{DES}\Delta}, 1\right) \tag{2.13}$$

F is a damping function in effort to force the solution towards RANS in boundary layers. The solution will then sway toward a RANS formulation in boundary layers where ϕ=1 but towards a LES solution when ϕ>1.

It shall be said that DES models such as the one mentioned above may not always work as expected. The intertwined use of many models and model constants may render the model too complex or even unusable for certain applications. Since the model "detects" the boundary layer automatically it might run in RANS mode in areas where one wants to capture fluctuations with LES. In the scope of this study it is inherent that the flow be treated in LES mode outside of at least 30 m ground distance because this is where the wind turbine rotor is situated. If flow is treated with RANS formulation above this it will render DES impractical in the scope of this study.

2.2.2 Surface roughness model

The lowest part of the ABL is called the surface layer. Wind in the surface layer is governed by the type of surface e.g, grass, trees, buildings, wavy oceans. Because it is computationally expensive to resolve this ground roughness with the mesh a model can be used instead. The velocity distribution below the roughness length is then modelled as:

$$u^{+}_{RH} = \frac{1}{\kappa} ln(\frac{y_0 + y}{y_0}) \tag{2.14}$$

Where y is the wall distance and y_0 is the roughness length. Increasing the roughness length will effectively result in the logarithmic region of the velocity profile to be closer to the wall. This model alleviates the need for very small vertical sizes of cells close to the wall in order to resolve the flow and in fact they should be kept an order magnitude larger than the roughness length used to produce physical results. Since this model uses a time-averaged expression of the velocity it is not possible to use this model directly with pure LES. Models such as DES where the wall layer is treated with RANS formulation makes it possible to use equation 2.14. This reduces the near wall resolution needed for DES and at the same time ensures proper wall layer modelling for ABL flows.

The dimensionless velocity u^+ is calculated through the use of the actual velocity (u) and the friction velocity (u_*) with the relation:

$$u^+ = \frac{u}{u_*}, \text{ where } u_* = \sqrt{\frac{\tau_w}{\rho}} \tag{2.15}$$

Where τ_w and ρ denote the wall shear stress and density, respectively.

2.2.3 Turbulent intensity

One way to quantify the turbulence of a flow is the measure of its turbulent intensity. Turbulent intensity varies between types of flows and can range from 10^{-2} for weakly turbulent inlets to 10^{-1} for strongly turbulent flows [21]. It is a dimensionless value expressing the fluctuations of the flow as a fraction of the mean velocity:

$$I = \frac{u'}{\langle u \rangle} \tag{2.16}$$

Since fluctuations are not resolved when using RANS simulations this quantity can be estimated using the turbulent kinetic energy in place of the fluctuation:

$$I \approx \frac{\sqrt{\frac{2}{3}k}}{\langle u \rangle} \tag{2.17}$$

2.2.4 Synthetic turbulence

In turbulent flow the kinetic energy content of large and small eddies varies. This is often presented with a function of turbulent kinetic energy versus wave number as shown in Figure 2.2. The wave number κ is inversely proportional to the eddy size so the left side of the graph shows energy for large eddies while eddy size decreases as we move to the right on the scale. In Figure 2.2 it is evident from the zone marked with Roman numeral "I" that the largest eddies contain most energy. In this regard the turbulent length scale denotes the size of these eddies. This is relevant because of how synthetic turbulence is generated at the inlet of DES and LES simulations. One of the ways *Star-CCM+* formulates the synthetic turbulence is to describe it by turbulent intensity (as outlined in section 2.2.3) and a turbulent length scale, i.e the size of the dominant eddies. These can be measured quantities or quantities estimated through other simulations. An estimate of the turbulent length scale can also be obtained through a precursor simulation. If using the k-ε model the relation to turbulent length scales is:

$$\ell_t \approx \frac{k^{3/2}}{\varepsilon} \tag{2.18}$$

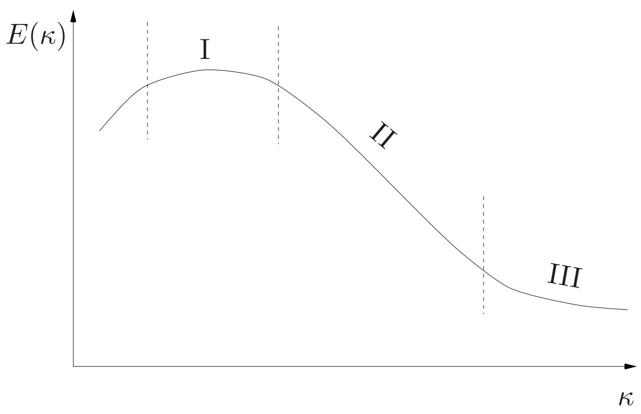

Figure 2.2: Energy spectrum of turbulent kinetic energy showing eddy wave number versus kinetic energy content, from [5].

2.2.5 Model application and computational grids

Discretisation schemes differ between RANS, LES and DES. This means that different critera apply when it comes to generating the computational grids. Lesser refinement is usually necessary in the near wall regions of RANS simulations compared to LES and cells can have high aspect ratios without causing problems. Since the boundary layers are treated with a RANS formulation in DES simulations the same critera applies to DES grids. In LES and the outer regions of DES, the filter width that separates the resolved turbulence from modelled one is scaled by the local grid size such that Δ=max(Δ_x,Δ_y,Δ_z). The least expensive way to keep the maximum grid spacing low (resolve as much as possible) is to use cubic cells (Δ_x=Δ_y=Δ_z). Therefore it is ideal that cells for LES have no stretching, i.e it should be dominated by cubic cells.

To resolve an eddy the grid size needs to be at least half of its turbulent length scale. By using the distribution of kinetic energy presented in Figure 2.2 the ratio of resolved scales can be estimated. Table 2.1 shows the approximate fraction of resolved kinetic energy versus ℓ_t/Δ [20].

Table 2.1: An estimate of the resolved turbulent kinetic energy versus grid size, from [20]

Resolved k $[k_{res}/k]$	**Grid size** $[\ell_t/\Delta]$
90%	12.5
80%	4.80
50%	1.25
10%	0.33

The surface roughness model is preferable for use in ABL flow and it makes the near wall refinement less costly. This potentially makes DES a preferable option over LES in the scope of this study. However DES might operate in RANS mode in areas close to the wind turbine which is unwanted. This problem of near wall turbulence dampening should not be a problem for LES. Because of the high Reynolds numbers encountered in the ABL it is highly impractical to expect LES to resolve turbulence in the immediate proximity to the ground. Given the size of turbulent length scales in the ABL it is however possible to resolve turbulence in the outer regions to a large extent.

It might prove difficult to argue the use of pure LES for flows such as the ABL mainly because in the absence of a wall roughness model it is too expensive to resolve the flow in the near wall regions. However if the flow is relatively well resolved in the outer layers it may prove useful to some extent. It is well achievable to resolve the outer layers with a resolution of about Δ=30 m. Since eddy length scales in the outer region may prove considerably larger than this, one might argue that the flow is relatively well resolved albeit only in the outer layers. As it is the interest of this project to investigate the effects of complex terrain on the turbulence, pure LES may still aid in drawing some conclusions even without the use of a rough wall model.

2.3 Blade Element-Momentum theory

Blade Element-Momentum (BEM) theory is a combination of two methods of examining flow past a rotor disk [9]. On one hand it is the calculation of elemental forces generated at the rotor blades (*blade element*) while at the other hand it is the conservation of momentum in an annular stream passing the rotor disk (*momentum*). By relating these two one can calculate the combined elemental forces generated on a wind turbine blade while on the same time maintaining the momentum balance over the rotor disk. Assuming that the wind field is a known function, the forces on the turbine blade can be calculated with acceptable accuracy at a relatively low computational expense.

Knowing the forces acting on all turbine blades means that many other quantities may be computed. These are for example: total power output of the wind turbine, structural moments or stress in various parts of the turbine and finally the dynamic responses of control systems.

2.3.1 Governing equations

An exact derivation of the BEM methodology is provided in [9] but it is only the governing equations which are presented here. Each blade element is ultimately exerted to forces that are determined through its lift (C_L) and drag coefficient (C_D). These coefficients vary with angle of attack but each elemental force is divided into parts parallel and perpendicular to the incoming flow. These forces are:

$$F_{x,el} = \frac{\rho A_{el} W^2}{2} \left(C_L\ sin\beta + C_D\ cos\beta\right) \tag{2.19}$$

$$F_{\theta,el} = \frac{\rho A_{el} W^2}{2} \left(C_L\ cos\beta - C_D\ sin\beta\right) \tag{2.20}$$

Equations 2.19 and 2.20 represent the forces of one single element but are used to sum up the total effect of the blades. The corrected flow angle β and corrected total flow velocity W come from:

$$tan\beta = \frac{\Omega r(1+a')}{V(1-a)} \tag{2.21}$$

$$W = \frac{V(1-a)}{cos\beta} \tag{2.22}$$

Where a and a' are axial and tangential induction factors, respectively. These induction factors act to conserve momentum over the rotor disk. They are deduced through an iterative process but the equations used to determine these induction factors are given by equations 2.23 and 2.24.

$$\frac{a}{1-a} = \frac{\sigma'[C_L sin\beta + C_D cos\beta]}{4Q\ cos^2\beta} \tag{2.23}$$

$$\frac{a'}{1-a} = \frac{\sigma'[C_L sin\beta - C_D cos\beta]}{4Q\lambda_r\ cos^2\beta} \tag{2.24}$$

Where σ', Q and λ_r denote the local solidity factor, tip loss correction factor and the local tip speed ratio, respectively.

2.3.2 Aero-elastic solver

By using the BEM methodology one can create solvers to predict wind turbine power output and dynamic responses. One such solver is the *FAST* solver developed by *The National Renewable Energy Laboratory* (NREL). It utilises the BEM method to assess the aerodynamic loads exerted on rotor blades. From the calculated aerodynamic loads other models are added to calculate blade deflections, required pitch angles, control signals etc. This forms a single comprehensive solver for wind turbine response. It shall be stressed that the quality of results depend on the quality of the wind field supplied.

2.3.3 Reference wind turbine

The wind turbine model used to assess the dynamic response is the *NREL 5-MW Baseline Wind Turbine*. It was developed as a representative model of a three bladed horizontal axis wind turbine. Its specifications come from publicly available properties from other projects that have been used to create a composite data set. The model is widely used as a reference in research work to quantify effects of various wind energy technologies of both land and sea based wind farms [10]. The main properties of the wind turbine are shown in Table 2.2.

Table 2.2: Properties of the NREL 5-MW Baseline Wind Turbine from [10].

Rating	5MW
Rotor orientation	Upwind, 3 blades
Control	Variable speed, collective pitch
Drive train	High speed, multiple-stage gearbox
Rotor, hub diameter	126 m, 3 m
Hub height	90 m
Cut-in, rated, cut-off windspeed	3 m/s, 11.4 m/s, 25 m/s
Cut-in, rated rotor speed	6.9 rpm, 12.1 rpm
Rating	5MW

To underline the benefits of using such a reference wind turbine, Figure 2.3 shows the operating conditions of the 5 MW reference wind turbine under steady state wind conditions. First and foremost is notable that the wind speed ranges from 3-25 m/s which is the operating range of the turbine. If the wind is below this limit the wind turbine will not generate any power (cut-in) and similarly if the wind exceeds this limit the blades will pitch to a feathered position and energy generation is ceased (cut-off). The output of this wind turbine is therefore regulated only with the use of blade pitch to control the rotor speed. This can be observed by the blue line which steadily increases with respect to wind speed until reaching its maximum at around 11 m/s from where it is constant with respect to wind speed. This is where pitching is initiated (shown with red line) which starts to grow from zero at around 11 m/s. Generator torque behaves similarly to the rotor speed as they are closely related variables because of the fixed gearbox.

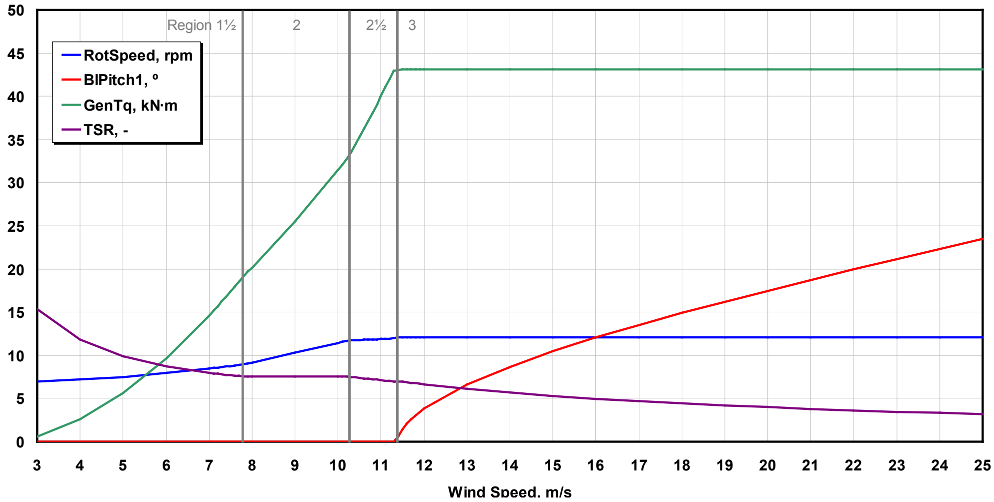

Figure 2.3: Steady state operational data for the 5 MW reference wind turbine, from [10].

2.4 Structural fatigue

Different load histories can be investigated in terms of fatigue without using specific component specifications and material properties. A way to achieve this is to use the *Equivalent Fatigue Load* (EFL). The EFL is calculated using [8]:

$$\mathrm{EFL} = \left(\sum_{i=1}^{n} \frac{S_i^m}{N_{eq}} \right)^{1/m} \tag{2.25}$$

Where S_i represents the load range of a cycle and N_{eq} represents any desired reference number of cycles. For calculations in this study the reference number of cycles is set to 600. The exponent m represents the logarithmic slope of the material's S-N curve (stress vs. amount of cycles until fatigue, also known as a Wöhler curve). Materials such as steel are common to be in the range of $2 < m < 3$ while composite materials have higher values. For this project m is taken to be 3 for steel and 10 for composite structures [13].

The EFL is independent of time history meaning that it does not care in which order loads are applied. It can not however be calculated directly from load histories, rather the time history must be analysed using methods such as the rainflow count to identify individual load cylces and their magnitude [1].

3

Method

This chapter explains in detail the methods used in this project and has been divided into separate sections covering the main parts. Using the information gathered from on-site measurements of wind (see Appendix A) the simulated wind direction and magnitude are decided to be 10 m/s from a direction of 216° with respect to the north. Since mean velocity can vary locally this reference velocity is measured at the met mast. The location of the met mast is shown in Table 3.1 among other important locations in the domain.

A computational domain is first generated using topography data from laser measurements of the area surrounding Rödbergskullen wind farm. The mean flow is then investigated using RANS for three reference velocities at the met mast. The results from RANS are then used to get an estimate of the turbulent length scale which is used for synthetic turbulence generation in DES/LES simulations. RANS simulations also reveal if there are any greater changes between velocities in ranges from 8-12 m/s. Transient simulations are carried out with both DES and LES models where instantaneous velocity data is extracted for use with the aero-elastic solver. Finally the turbine response is simulated with the aero-elastic solver with flow over flat and complex terrain. All CFD simulations are carried out using the commercially available *Star-CCM+* solver while aero-elastic simulations are carried out using the open-source *FAST* solver from *NREL*.

3.1 The computational domain

Two computational domains are generated, one consisting with ground generated to match the terrain around Rödbergskullen and one where the ground is absolutely flat. They have been dubbed the complex domain and the flat domain throughout the remainder of this report. Since other factors of both domains are identical only the details of the complex domain are covered here.

The domain is constructed such that the inlet is perpendicular to the simulated wind direction (216°). It is essentially a rectangular box with all sides flat and parallel to each other except the floor which is made up of the topography of the area. The domain is shown in Figure 3.1 where the inlet boundary is marked in red while the outlet is marked in orange. The coordinate system is such that the y-axis is vertical, x-axis is acting parallel to the wind direction and the z-axis perpendicularly. The vertical extent of the domain is such that it reaches 1500 m above the highest point on the ground. The streamwise length of the domain is 10 km while the spanwise width is 6.5 km. The centre of the domain is a point in the middle of the Rödbergskullen wind farm close to the met mast which is used to scale the study. This ensures that flow structures can develop before reaching the area of interest but the effects of flow structures downwind are also captured. The coordinates of the central point, met mast and wind turbine to be studied are shown in Table 3.1. Their locations are provided both in terms of SWEREF 99 but also in the local coordinate system of the domain. From the local coordinate system we see that the centre of the domain is the origin but the met mast and wind turbine are located close by.

Table 3.1: Positions of important locations in the domain.

	SWEREF 99	(x,z) m
Centre of domain	N 6682821.00, E 457085.00	(0,0)
Met mast	N 6683430.11, E 457058.24	(477,-379)
Wind turbine No. 1	N 6683515.63, E 457022.21	(525,-459)
Wind turbine No. 2	N 6683211.26, E 457226.85	(399,-115)
Wind turbine No. 3	N 6683002.67, E 456844.56	(6,-301)
Wind turbine No. 4	N 6682839.94, E 457434.30	(221,271)
Wind turbine No. 5	N 6682634.43, E 456895.03	(-263,-44)
Wind turbine No. 6	N 6682554.50, E 457224.88	(-133,270)
Wind turbine No. 7	N 6682403.92, E 456355.07	(-776,-345)
Wind turbine No. 8	N 6682151.38, E 456874.95	(-665,223)

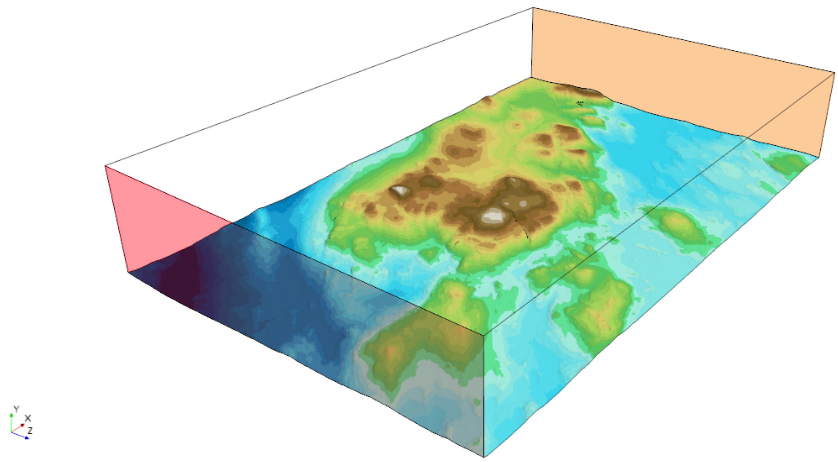

Figure 3.1: The computational domain is a rectangular box with the floor being the topography of the site. Vertical surfaces marked in red and orange are the inlet and outlet, respectively. The inlet is aligned perpendicular to the simulated wind direction, 216°.

3.1.1 Topography

Laser measurements of the ground obtained from *The Swedish University of Agricultural Sciences* (www.slu.se) has been imported to *Globalmapper* (software) to provide the topography of the site on the form of an STL file. The STL file has then been imported to *Star-CCM+* in order to generate the domain. This data is resolved with a resolution of 7 m. This secures that large structures in the terrain are captured while smaller ones like trees and houses etc., are filtered out. When turbulence models allow these smaller structures are modelled by a surface roughness length, y_0. Since the area is covered partly by farmlands and partly by dense forest the surface roughness factor will in reality differ from place to place. However the approach taken in this project is to model the whole domain floor with the same universal roughness length.

3.1.2 Mesh

Since the mesh requirements and practices between different turbulence models differ, two meshes are generated for each type of domain (flat/complex). For RANS simulations the mesh consists of approximately 23 million cells with a constant horizontal cell resolution of 30x30 m. Vertical distribution is such that cells are small close to the ground but eventually reach 30 m. The first 50 cells adjacent to the ground have a cell height of 2 m and after that they grow with a constant rate eventually reaching 30 m vertical size at a height of 250 m a.g.l. The first cell height of 2 m is dictated by the use of the roughness length and the fact that in order to get physical results the first cell height needs to be an order magnitude larger than the roughness length ($y_0 = 0.2$ m).

For the DES simulations the mesh is somewhat different due to the fact that calculations are transient. The transient nature results in a substantial increase in the amount of iterations needed and therefore longer computational times. This raises a requirement to dramatically lower cell count when compared to RANS. The mesh for DES has a base size of 30 m cubic cells but the vertical distribution is altered close to the ground. The cells adjacent to the ground have a vertical height of 2 m and grow in size vertically to eventually reach the global 30 m size at an altitude of 60 m. This mesh is somewhat similar to what has been used with good results in previous work albeit using the hybrid LES-RANS model instead of DES [3]. The final cell count of the mesh is approximately 4.4 million. This mesh is also used with LES because of limits on computational time.

3.2 RANS simulations

The RANS simulations provide a platform to scale inlet conditions to reach preferred reference wind speeds at the location of the met mast. Since the simulations are of a neutral atmosphere, temperature, viscosity and pressure are chosen to be uniform throughout the domain. Their values are taken from the *International Standard Atmosphere* (ISA) at an elevation of 1000 m. The chosen inlet conditions are those of a neutral ABL wind profile with constant shear stress. The prescribed quantities at the inlet are velocity (u), turbulent kinetic energy (k) and dissipation (ε). Their values are computed from the dimensionless friction velocity u_* using equations 3.1-3.4 [4][14]:

$$u_* = \kappa u_{ref}\ log^{-1}(\frac{y_{ref} + y_0}{y_0}) \tag{3.1}$$

$$u(y) = \frac{u_*}{\kappa}\ log(\frac{y + y_0}{y_0}) \tag{3.2}$$

$$k = \frac{u_*^2}{\sqrt{C_\mu}} \tag{3.3}$$

$$\varepsilon(y) = \frac{u_*^3}{\kappa(y + y_0)} \tag{3.4}$$

Where y_0 denotes the roughness length, κ is the von Karman constant and C_μ is a model constant. Note the "(y)" notation in equations 3.2 and 3.4 indicates that these equations are functions of y while the dimensionless friction velocity and turbulent kinetic energy in equations 3.1 and 3.3 are constant with altitude. The reference velocity (u_{ref}) and reference altitude (y_{ref}) will in combination make the velocity profile pass through the desired velocity at the desired altitude.

Table 3.2 contains a summary of the boundary conditions used in the RANS simulations. The sides refer to the lateral sides of the domain while the ceiling is the top surface of the domain. The roughness length (y_0) is set to be 0.2 based on the terrain consisting mainly of tall trees with some patches of flat grasslands [19].

Table 3.2: Overview of the boundary conditions in the RANS simulations.

Boundary	**Type**	**Defined quantities**
Inlet	Velocity inlet	u,k,ε
Outlet	Pressure outlet	p=0
Ground	Rough wall	y_0=0.2
Ceiling	Symmetry plane	-
Sides	Symmetry plane	-

Three reference velocities (8, 10 and 12 m/s) are simulated with RANS to investigate if there are any considerable changes noticeable between such velocities. The reference velocities are measured at the met mast location at an altitude of 60 m. To obtain these velocities at the met mast the inlet reference values are tuned. These inlet reference values are listed in Table 3.3.

Table 3.3: Overview of the inlet boundary reference values.

Wind speed	u_{ref}	y_{ref}
8 m/s	5.4	50
10 m/s	6.7	50
12 m/s	8.0	50

The RANS simulations utilize a steady, constant density, realisable k-ε model with altered constants to simulate the ABL. The constants used are shown in Table 3.4 [2]. The solver is segregated with second order spatial discretisation schemes.

Table 3.4: Overview of the k-ε model constants used.

Constant	κ	C_μ	$C_{\varepsilon 1}$	$C_{\varepsilon 2}$	σ_k	σ_ε
Value	0.40	0.03	1.21	1.92	1.0	1.3

3.3 DES and LES simulations

The DES and LES simulations provide a transient description of the flow field. Transient simulations are calculated only for for a mean wind speed of 10 m/s at the met mast. Pressure, temperature and viscosity are identical to those used in RANS. The use of wall roughness modelling is applied to DES simulations while it is omitted for LES since no such option is available through *Star-CCM+*. This makes the LES simulations somewhat "incorrect" and by using the same mesh as for DES perhaps hard to justify. However it is a comparison of the fluctuating quantities between flat and complex terrain that is of interest and given the large turbulent scales present in the outer layers of the ABL the outer layers are likely to be relatively well resolved.

The DES model was described shortly in section 2.2.1.3 and the LES with Smagorinsky Subgrid Scale model was described in section 2.2.1.2.

Turbulence at the inlet is synthesised using the description of the mean velocity profile given by equation 3.2 together with turbulent intensity and a turbulent length scale. The turbulent intensity is taken from the approximate turbulent intensity measured at the met mast (13% as seen in Appendix A) while the length scale is taken from the previous RANS results using equation 2.18. To limit computational time of synthetic eddies, a constant length scale of 50 m is assigned below an altitude of 15 m. Lower values result in many more eddies being computed at the boundary, slowing down the simulation. Since the flow is incompressible the synthetic turbulence is scaled in order to keep a constant mass rate moving across the boundary. An overview of the prescribed boundary conditions in DES/LES is shown in Table 3.5

Table 3.5: Overview of the boundary conditions used for the DES and LES simulations.

Boundary	Type	Defined quantities
Inlet	Velocity inlet	u,I,l_t, synthetic turbulence.
Outlet	Pressure outlet	p=0
Ground	Rough/smooth wall	y_0=0.2 for DES/Smooth wall for LES.
Ceiling	Symmetry plane	-
Sides	Symmetry plane	-

Time discretisation is second order implicit with a time step size of 50 ms. This timestep is chosen to speed up convergence but also since the aero-elastic solver dictates that the timestep be of this order. In fact the structural time step of the aero-dynamic solver is an order magnitude smaller but having a much smaller time step for the CFD will be unlikely to resolve an increased amount of fluctuations because of the chosen grid size.

For a mean wind speed of 10 m/s an approximate flow pass takes 1000 s. After one flow through, the sampling for time-averaged velocities and Reynolds stresses is initiated. The total simulation time is 2000 s. Only one turbine is studied and therefore data is only collected for one turbine. A sampling grid is located at wind turbine No. 8 location and velocity data is collected for the last 10 minute period. The coordinates of the wind turbine is shown in Table 3.1. This sampling grid is parallel to the inlet and spreads from 15 m height to cover an area of 200x200 m^2 in order to fully cover the rotor diameter. Data of instantaneous velocity components on the sampling grid are collected at every time step.

3.4 Aero-elastic simulation

To assess the wind fields effect on the dynamic response of a wind turbine, the wind data generated with CFD is used as an input for the *NREL FAST* aero-elastic solver. The wind turbine model used is based on the *NREL 5-MW Baseline Wind Turbine* as described in section 2.3.3. The structural time step is 6.25 ms while the aerodynamic time step is 50 ms.

The assigned inital state of the simulated wind turbine (e.g rotational speed) can cause large fluctuations of data in the beginning of a simulation until the wind turbine adapts to the provided wind field. To prevent these fluctuations affecting the studied results the initial 1000 s of aero-elastic simulations are carried out with the wind field frozen on the first time step. This eliminates the fluctuations from the collected data.

The total simulation time is 10 minutes and results for the turbine response is collected at every time step. Effects of the tower on the wind field is neglected.

4

Results

The results are presented in the order of which they are attained. Since it is mainly the vicinity of the wind turbine that is of interest the results are only shown for the lowest 250 m of the domain. Marked specially on the height axis of figures are the altitudes of 30 and 150 m which coincide with the bottom and the top of the rotor disk but also marked is the height of 90 m which is the hub height of the wind turbine. In section 4.1 are presented the the effects of complex terrain on the mean flow field evaluated by RANS. Following this is section 4.2 where the time-averaged results from DES/LES are compared to RANS. The DES model did not resolve an adequate amount of turbulence in the proximity of the wind turbine and so it was not used to assess the turbine response. A brief look at the transient flow field generated by LES is then covered in section 4.3 and finally the response of the wind turbine using the wind field generated by LES is shown in section 4.4.

4.1 RANS over flat and complex terrain

The time-averaged results provide a sound description of how the flow field looks like under neutrally stratified conditions. A comparison has been made of the flow over complex and flat terrain using the same boundary conditions, highlighting the effects the terrain has on the flow. In Figure 4.1 the velocity magnitude profiles versus height above ground are shown. The legend shows entries marked with "c" and "f" but these denote the shape of the terrain (*complex* or *flat*). The position of the data shown is the met mast location. The reference velocities of 8, 10 and 12 m/s are those at 60 m above ground as can be seen from the solid lines. From Figure 4.1 it is evident that the wind has a relative speed-up when comparing the complex terrain results with those of flat terrain. This is to be expected just as previously explored in section 2.1.2 and perhaps this can be taken (at least partially) as an indicator that these simulations are of good quality.

In the inner regions ($y < 150$ m) the velocity increase between flat and complex terrain is around 20% in all cases but surprisingly the outer regions ($y >> 150$ m) also exhibit a velocity increase. This outer region velocity increase is however minimal but should be kept in mind when later drawing conclusions. Perhaps this outer region velocity increase is due to the incompressible nature of the simulations, forcing a total speed-up of the flow past the mountain.

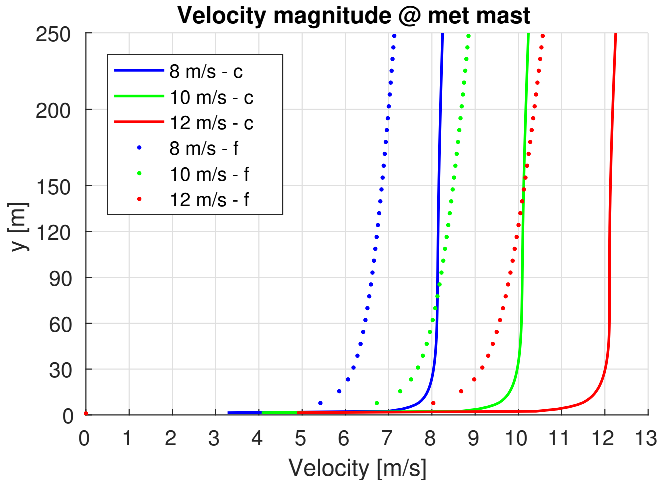

Figure 4.1: Comparisons of RANS generated velocity profiles. Legend entries with "c" or "f" refer to complex and flat terrains, respectively.

The inlet for RANS simulations are assigned with constant values of turbulent kinetic energy with altitude but as the flow develops inside the domain, turbulent kinetic energy is quickly distributed unequally with respect to the altitude. The turbulent kinetic energy profile at the met mast location is shown in Figure 4.2 both over flat and complex terrains. All vertical profiles of turbulent kinetic energy essentially have the same shape although there are differences in their magnitudes. The profiles over the complex terrain have higher turbulent kinetic energy when compared to those profiles simulated over flat terrain. This increase is largest in the lowest regions. This seems natural as there is more turbulence present on a mountain top than over flat plains.

A similar trend is seen in Figure 4.3 where the turbulent dissipation rate is shown at the met mast. The dissipation rate is larger for higher wind speeds which can be expected since the applied inlet conditions govern this to a large extent and the fact that the added turbulence causes more dissipation to occur. The added turbulent kinetic energy causes a change such that dissipation is slightly higher where turbulent kinetic energy has increased and vice versa.

As for turbulent intensity the results for all wind speeds are identical. These results are shown in Figure 4.4. There is only a change between complex and flat terrains. This is because the chosen inlet conditions are derived with the assumption of constant shear stress with no regard to turbulent intensity levels. Also the approximated quantity of turbulent intensity (equation 2.17) compares the turbulent kinetic energy to the mean velocity, both of which increase with increased wind speed. The complex terrain however, reduces the turbulent intensity as is seen in Figure 4.4. This is contrary to what, at least in the author’s opinion, is expected through plain intuition. One reason for this is seen in Figures 4.1 and 4.2 as the increase in velocity over complex terrain is far greater than the increase in turbulent kinetic energy. It is not the scope of this project to accurately describe the changes in turbulent intensity through RANS simulations and therefore this is not of relative significance. The turbulent intensity predicted by RANS over complex terrain is 9%. This is close to the measurement over Rödbergskullen (13% as seen in Appendix A). The met mast anemometer only measures wind speeds in the horizontal plane so the vertical component gets filtered out. This vertical component can be expected to be relatively small compared to the axial and lateral components so close to the ground and therefore the turbulent intensity as expressed by the anemometer is likely to be larger than actual values.

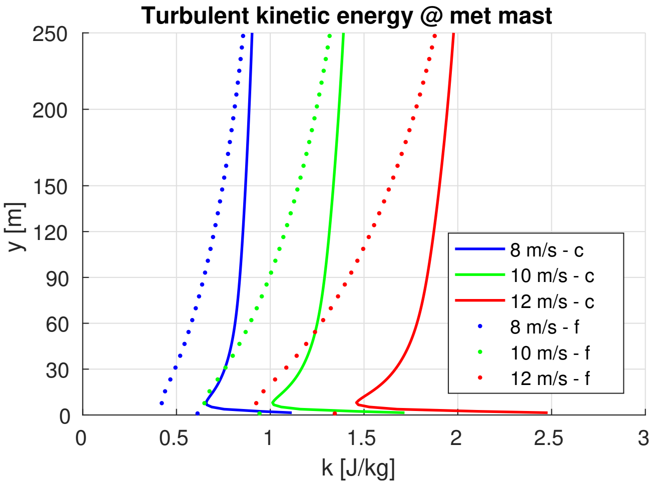

Figure 4.2: Comparison of turbulent kinetic energy profiles from RANS simulations. Legend entries with "c" or "f" refer to complex and flat terrains, respectively.

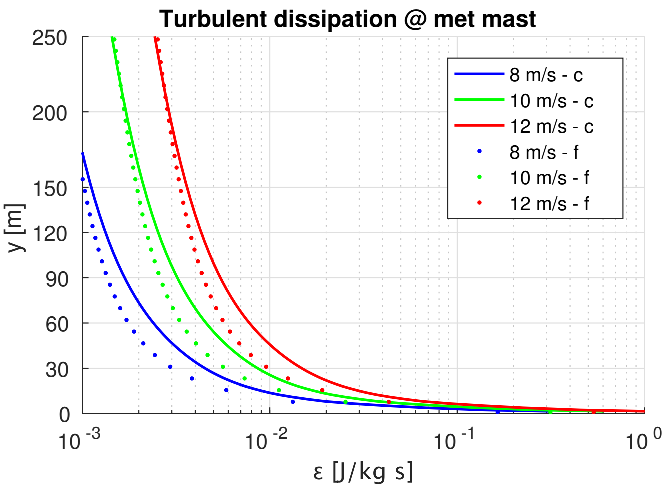

Figure 4.3: Comparison of turbulent dissipation profiles from RANS simulations. Legend entries with "c" or "f" refer to complex and flat terrains, respectively.

The turbulent length scales as quantified by equation 2.18 are shown in Figure 4.5. The values are calculated on a vertical line at the centre of the flat domain and are used as inlet conditions for DES/LES simulations. The increase in length scale with altitude is linear except in the immediate proximity of the wall where it deviates

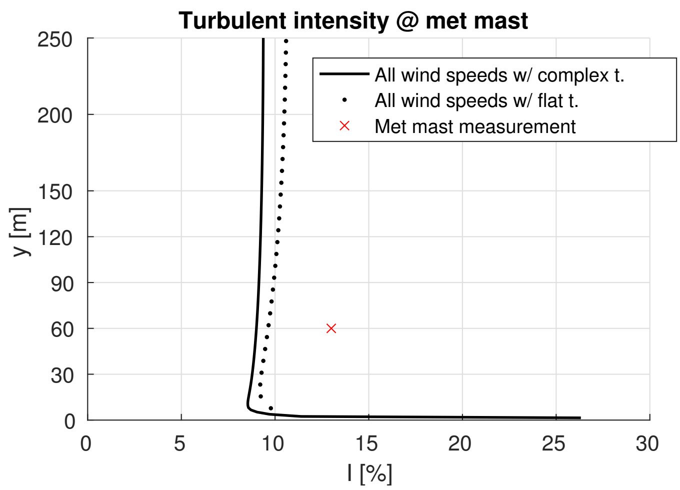

Figure 4.4: Comparison of turbulent intensity profiles from RANS simulations. All velocities simulated generate the same results.

slightly from a linear path. Turbulent length scales are fairly large when compared to the dominant cell size of 30 m with almost 7 cells covering the largest eddies at a height of 50 m. Investigating the level of resolved scales for later LES one can divide the length scale with 30 m to get the scale shown on top of Figure 4.5. Comparing this scale to Table 2.1 it is evident that the fraction of resolved turbulent kinetic energy can be expected to be well above 90% in most of the domain. It is only in a region below approximately $y < 50$ m that the level of resolved turbulence will fall below about 80%. In the region below 15 m more than 50% of the turbulence is modelled. Worth noting is that this region of relatively little resolved turbulence ($y < 15$ m) is located below the turbine rotor plane.

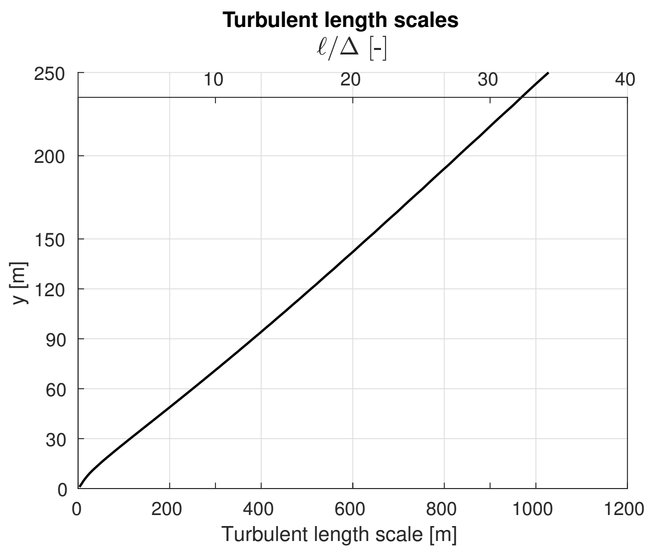

Figure 4.5: Turbulent length scale estimates from RANS used for synthetic turbulence generation for DES/LES. The bottom horizontal axis refers to the turbulent length scale (ℓ) while the top horizontal axis refers to the turbulent length scale over grid size (Δ). The top horizontal axis can be used to estimate the amount of resolved turbulence by comparing to Table 2.1.

4.2 Time-averaged LES/DES

The mean velocity profiles attained through DES and LES are compared with those attained through RANS in Figure 4.6. Studying the profiles over flat terrain, DES captures the shape of the RANS profile although it has somewhat lower velocities. This may be explained with the fact that although the DES has similar RANS formulation in the boundary layer it is based on a SST-k-ω model rather than the k-ε used for the precursor RANS simulations. LES gives average velocities that lie closer to the RANS profile than DES. The variation where it is largest is approximately 5%. LES also captures well the velocity profile expected for the complex domain. This points to the fact that even without the roughness model of the ground, LES seems to do an outstanding job of capturing the velocity profiles. It may be that compared to the scales of the complex geometry (hills and valleys in the range of 100 m) the roughness of the ground plays only a minor roll. For the LES of complex terrain there is however an unnatural change in velocity at roughly 150 m that indicates that the time taken to average the velocity was not long enough. This is an observation seen in other parts of the results as well.

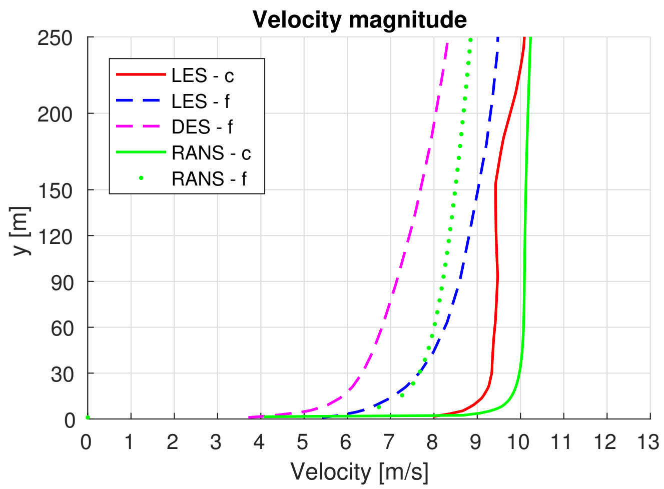

Figure 4.6: Velocity magnitude profiles compared. Dashed and dotted lines denote flat terrain whilst solid lines indicate complex terrain.

It is not only important to capture the mean velocity profiles well because it is imperative that the turbulent kinetic energy of the transient results match that which is predicted through RANS. Shown in Figure 4.7 is the resolved turbulent kinetic energy for both DES and LES simulations. Limits of the DES for the scope of this project are now clearly seen as the resolved turbulent kinetic energy (captured fluctuations) is much lower than what is predicted through RANS. The resolved turbulent kinetic energy in the outer regions might be satisfactory but it should be kept in mind here that the wind turbine rotor extends from about 30 m to 150 m. In this height range the resolved turbulent kinetic energy of the DES gradually decreases to zero, indicating that this section is being treated with RANS formulation. Studying the profiles generated by LES for flat and complex terrains they are not an exact match with the RANS results although they are close. The trend is similar too in both cases. Yet again the profiles are showing evidence that the time over which they are sampled is not long enough.

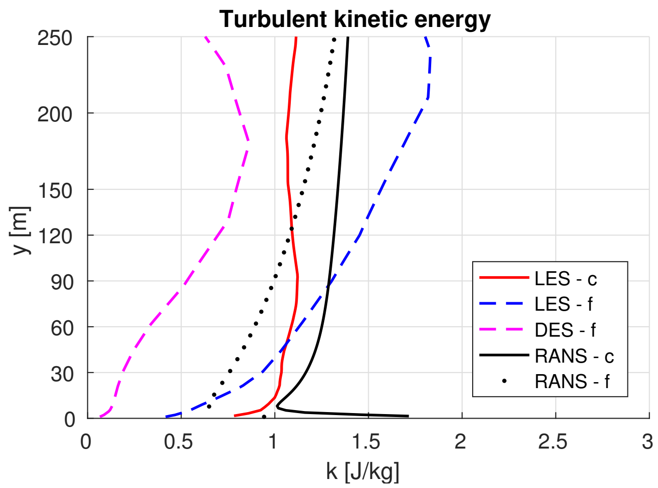

Figure 4.7: Resolved kinetic energy of DES and LES simulations compared to that predicted by RANS. Dashed and dotted lines denote flat terrain whilst solid lines indicate complex terrain.

To put the resolved turbulent kinetic energy into perspective it is compared to the time-averaged velocity to form turbulent intensity. The resolved turbulent intensity is shown in Figure 4.8. Studying the DES results it underlines its limits to provide a transient model of the ABL for use with the aero-aelastic solver. The LES results for both flat and complex terrains match well with the RANS results. From Figure 4.8 one can also see that the roughness model in RANS which seeks to increase turbulence close to the ground is missing from the resolved LES. This increase is however far below 30 m and thus it does not affect the aero-elastic solver used to assess the wind turbine response directly.

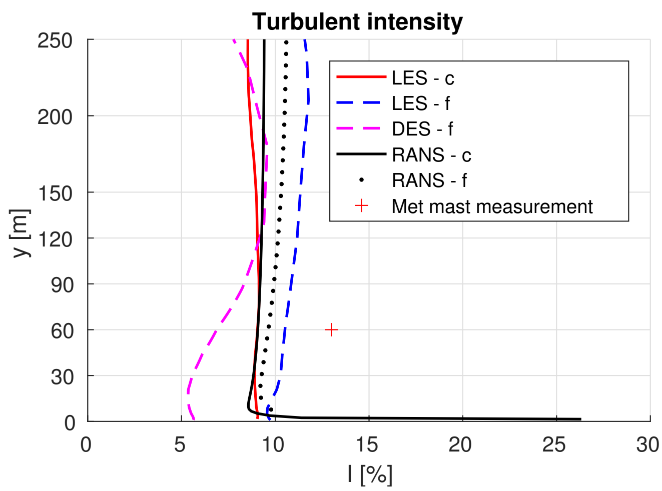

Figure 4.8: Turbulent intensity of RANS, DES and LES compared. Also shown in the figure is the measured average on Rödbergskullen. Dashed and dotted lines denote flat terrain whilst solid lines indicate complex terrain.

So far the resolved turbulence has only been presented as a summation of the individual three dimensional components. To better understand the behaviour of the flow one can study the individual stresses i.e the Reynolds stresses. From here on DES results are omitted since they are not used in any further investigation for this study.

Shown in Figure 4.9 are the Reynolds stresses of the LES. On the left side normal stress of the flat and complex domain are shown while on the right side the shear stress. Solid lines denote the complex domain while broken lines denote the flat domain. Studying the dashed lines of Figure 4.9 the normal stress in the streamwise direction $<\overline{u'u'}>$ is not the largest as can be expected in simple channel flow. Rather the cross component $<\overline{w'w'}>$ is largest. The setup of the domain is similar to large scale channel flow although the true nature of the wind can perhaps not be viewed as such. It seems however logical that for the flat domain the streamwise component of fluctuations should at least match those of the crosswise fluctuations. This points towards that the sampled time span is not descriptive of the fully developed flow. Also similar to channel flow, components in the vertical direction $<\overline{v'v'}>$ starts from zero at ground level and gradually grow with altitude. The change brought on by the complex domain is a strong decrease in both $<\overline{u'u'}>$ and $<\overline{w'w'}>$ except in the lowest 50 m where $<\overline{u'u'}>$ grows considerably. The vertical component almost doubles in magnitude for the complex domain as compared to the flat domain. While the outer layers of the LES are very well resolved one can not expect the changes in normal stresses to be physical in the lowest part of the domain as the flow is not well resolved here. Furthermore it is difficult to summarise all these changes of normal stress behaviour into one sentence but to give it a try the main trend for changes in normal stresses is a growth in vertical components and a decrease in stream and cross wise components.

In channel flow all shear stresses can be expected to be zero (assuming fully developed flow) except for the $<\overline{u'v'}>$ component. However this can be seen neither from the flat or the complex domain simulations. Perhaps the reason for this is that the lowest part of the domain is not well resolved causing a lack of information of the ground to affect the outer regions of the flow. On top of this the absence of a rough wall model might be at least part of the explanation here. There is then a similarity between flat and complex domains where $<\overline{u'w'}>$ component is non-zero. For the complex domain the reason for this is that the time-averaged w velocity is non-zero due to the presence of the mountain. However this can not be used as reasoning for the flat domain and thus it points yet again to the fact that perhaps a longer sampling time is needed.

The somewhat unexpected behaviour of turbulent stresses is worth a closer investigation. Shown in Figure 4.10 are the resolved Reynolds stresses of the complex domain over a wider span of altitudes than in Figure 4.9. The shear stress is found to be non-zero in large parts of the domain but since this is the complex terrain where the flow can locally be altered in horizontal directions this is perhaps difficult to criticise. However by studying the normal stresses it shows a strong drop to zero at altitudes above 700 m. For the vertical fluctuations this is most certainly caused by the symmetric boundary imposed at the ceiling of the domain. Since the

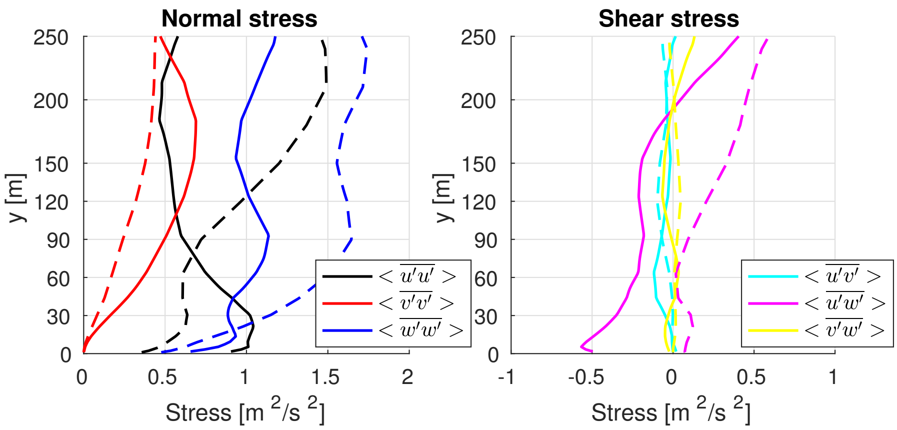

Figure 4.9: A comparison of resolved turbulent stress from LES with flat and complex terrain. Dashed lines denote flat flat terrain whilst solid lines indicate complex terrain.

turbulent length scale assigned at the inlet grows with altitude the large eddies at higher altitudes are dampened by the presence of the symmetric boundary. Because length scales at these high altitudes are large the drop in lateral fluctuations might also be related to a too short sampling time. All this may affect the simulation as a whole in a negative way although transient data from far below 700 m is used to asses wind turbine response.

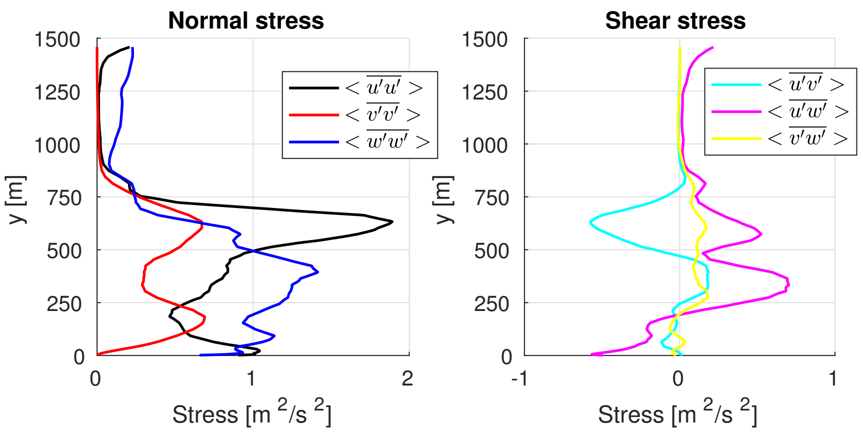

Figure 4.10: A comparison of resolved turbulent stress at high altitude from LES with complex terrain. The low vertical normal stress at altitudes above 500 m demonstrates the effect of symmetric boundaries on fluctuations. The low lateral normal stress could point toward longer sampling times needed to capture stresses.

4.3 Transient LES

To get a sense of the time dependant behaviour of the LES one can look at box plots of the wind components u, v and w. The boxplots show the sample median as a red line, blue lines at the 25th and 75th percentiles of the sample and finally a black line denoting the ends of the interquartile ranges. Samples outside of the interquartile range (outliers) are marked as red crosses. Figure 4.11 shows this box plot for the three wind components at hub height of the wind turbine over the period of 600 s which is used to assess the wind turbine response. Starting with w its distribution is near identical between flat and complex terrain the only difference being a slightly larger spread and the presence of a few outliers for the complex terrain. The median is not located at zero for the complex terrain and this only underlines the fact that the presence of the hill alters the governing wind direction slightly locally. A similar behaviour is seen when looking at the v component where the overall spread is similar for both flat and complex domains while there is a shift from the medians location away from zero for the complex domain. This is expected as the presence of the hill deflects the mean flow upwards on the windward side and slightly downwards at the leeward side as the wind flows past Rödbergskullen. When studying the stream wise component u, there is great difference between flat and complex terrain. While the medians of the flat and complex domains are located only 1 m/s away from each others there are numerous outliers located in the top range of the complex domain. This indicates a greatly skewed distribution and perhaps the presence of a gust or a short period of high velocities in the sample.

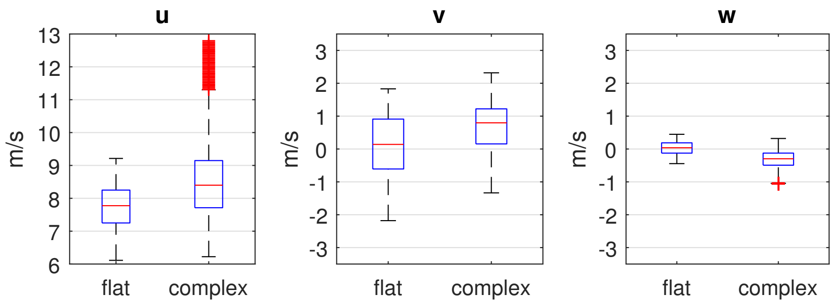

Figure 4.11: Boxplot distributions of wind components at hub height. u is the streamwise component, v the vertical and w the crosswise component.

For a deeper investigation the time histories of velocity components at hub height are shown in Figure 4.12. Here it can be confirmed that indeed components of v and w behave similarily over flat and complex terrains. Studying the time history of u however reveals that the first 500 s the behaviour is somewhat similar over flat and complex terrains but in the last minute or so there is a large peak showing over the complex terrain. This indicates that although the time-averaged wind velocity of the complex domain is considerably higher than over flat terrain its nature seems to be such that it fluctuates around a similar mean value as over flat terrain with the time-averaged value then being increased significantly by the passing of high velocity gusts. However it is perhaps not wise to draw such conclusions since previous results show that longer times should be used to time-average the flow. Another thing to take from Figure 4.12 is the absence of any higher frequencies in the wind. This is most certainly because of the grid size used is filtering out the higher frequencies (i.e smaller eddies).

It is fortunate that the u component gust occurs at the end of the simulation since no efforts are made to save the global fields of velocity for later investigation. The last time step is however saved and is shown in Figure 4.13. This is approximately

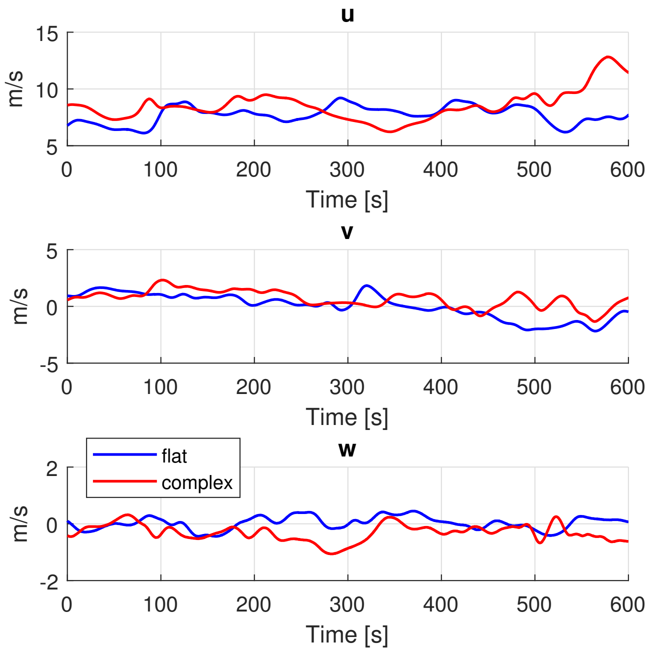

Figure 4.12: Time histories of wind components at hub height. u is the streamwise component, v the vertical and w the crosswise component.

30 s after the peak of the gust passes the wind turbine. Seen in Figure 4.13a is the location of the wind turbine and behind it is the patch of high velocity indicating the presence of the gust. Also in the lee of the mountain are (or what seem to be) two or three periodic separations (patches of blue). For comparison a similar image is shown for the flat domain in Figure 4.13b where neither a large gust nor large separations are visible.

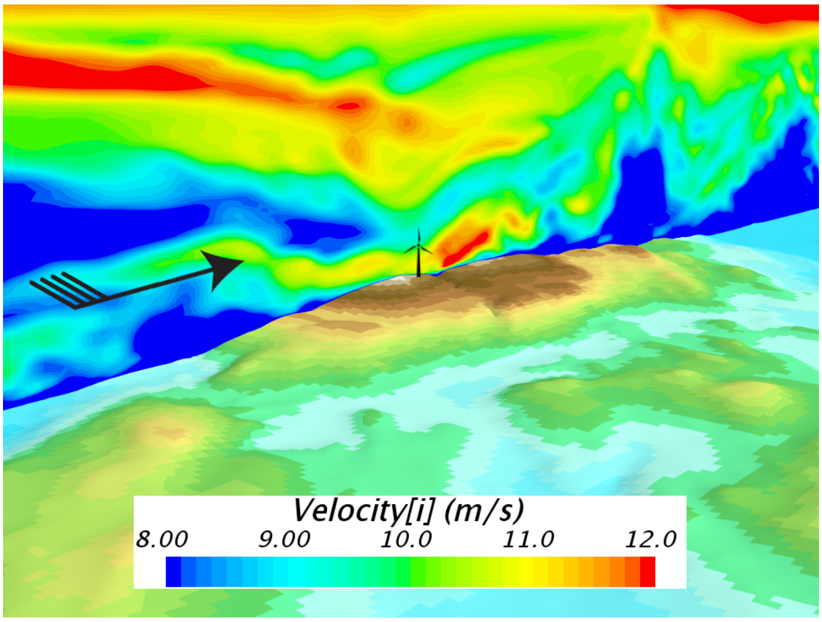

(a)

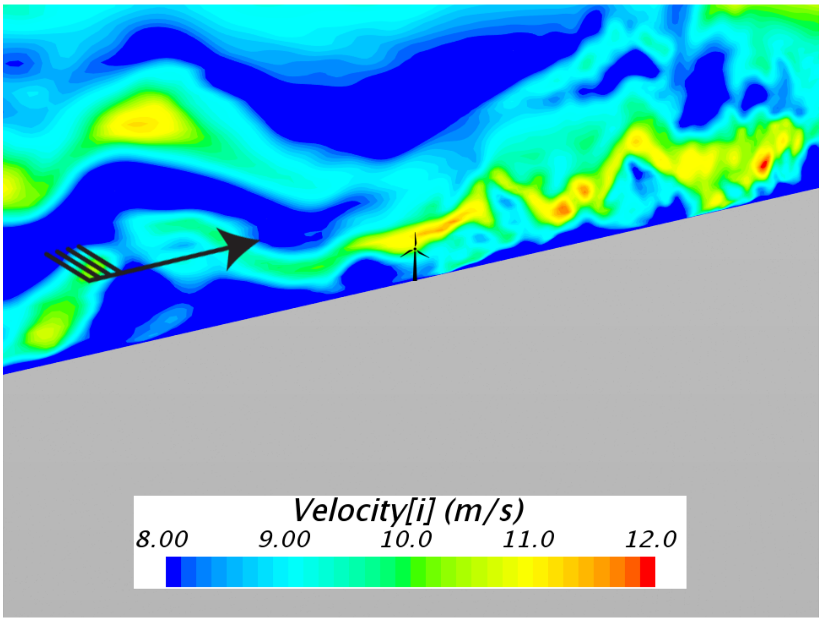

(b)

Figure 4.13: Instantaneous velocity field u at a streamwise plane at t=2000 s. Wind turbine is shown with exaggerated scale of 1.5 for clarity and the arrow marks the incoming wind. Seen in (a) is the red patch associated with the passing of a 13 m/s gust just downstream of the wind turbine.

4.4 Wind turbine response

Only the wind fields generated with LES are used to assess wind turbine responses since the DES results do not achieve a sound enough representation of the transient fluctuations in the vicinity of the wind turbine. This makes for two response results.

A response of a wind turbine situated on Rödbergskullen when the wind measures approximately 10 m/s at the met mast (complex terrain simulation) and a response of a turbine situated in a flat domain using the same boundary conditions as the complex terrain simulation.

There are four variables which have been chosen for the investigation of the turbine response. The first of these is the torque exerted on the low speed gearbox shaft which has been abbreviated to GBXTQ. The torque acting on the gearbox shaft is important since it gives an idea of the forces acting directly on the gearbox. The second of these parameters is the fore and aft bending moment acting on the tower base, abbreviated TBFAM. Fore aft bending moment is expected to fluctuate but if the change in streamwise fluctuations are large when comparing flat and complex terrains TBFAM will be greatly affected. The third variable is the flapwise bending moment at the root of a rotor blade, abbreviated FWBM. Since it is important to study the various different parts of the wind turbine, FWBM can perhaps be a preferable gauge on how the complex terrain affects turbine blades. The fourth and final parameter studied is the bending moment acting on the low speed shaft, abbreviated LSSBM. The bending moment of the low speed shaft is interesting as it is experienced at the main bearing of the wind turbine rotor shaft. The variables and their abbreviations have been collected into Table 4.1.

Table 4.1: Abbreviations of studied variables of the turbine response.

GBXTQ	Gearbox shaft torque
TBFAM	Tower base fore aft bending moment
FWBM	Rotor blade bending moment at root
LSSBM	Low speed shaft bending moment

Shown in Figure 4.14 is the rotor speed, gearbox shaft torque and collective pitch as functions of time for both flat and complex terrains. Because the wind turbine encounters the predominant wind direction both rotor speed and gearbox torque behave much similar to the u component in Figure 4.12. Pitch is only used to regulate operations to stay below rated conditions of 12.1 rpm rotor speed and so it is not needed for the flat domain and only for a short period in the complex domain. This activation of the pitch control causes a hacksaw like shape in the values for gearbox torque undoubtedly causing an increased fatigue of mechanical parts.

The amount of fatigue is difficult to express when presenting loads as time dependent functions. Rather than looking at the time dependent gearbox shaft torque it can be presented as a boxplot as seen in Figure 4.15. The difference between flat and complex terrains mainly lies in a larger spread of values within the complex domain and more importantly the presence of frequent outliers in the torque caused by the gust of wind covered in section 4.3.

Examining the time history of torque using a rainflow count one can identify the number and magnitude of the exerted load cycles. The results are shown in terms of a histogram in Figure 4.16. The histogram underlines the similarity between the

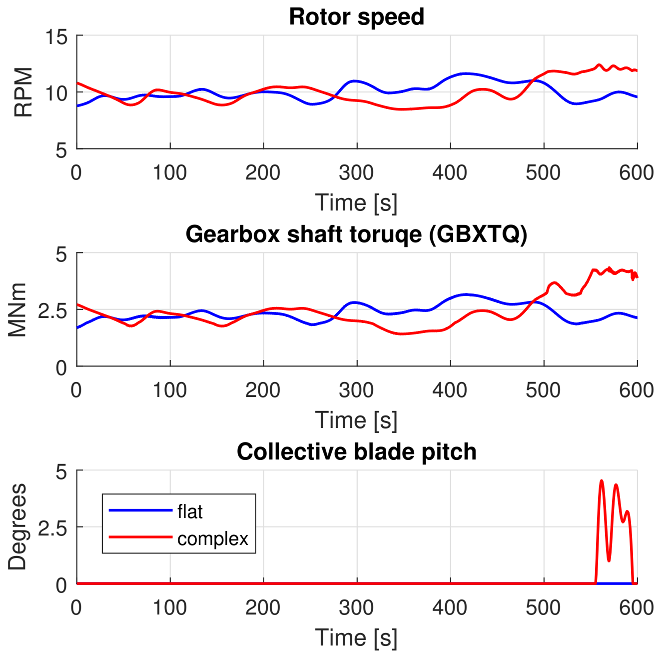

Figure 4.14: Time histories of rotor speed, gearbox shaft torque and collective pitch angle.

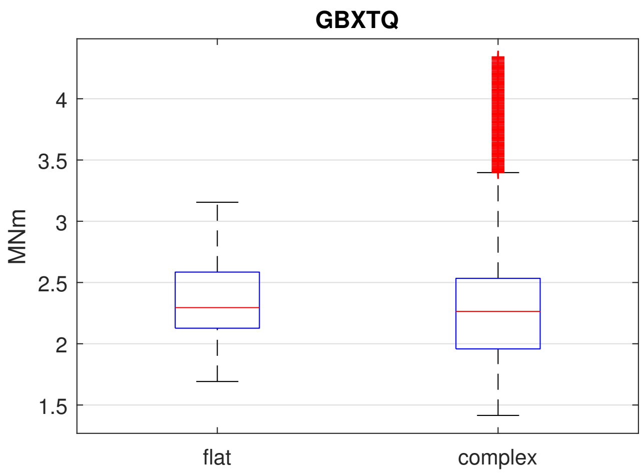

Figure 4.15: Boxplot distribution of gearbox shaft torque. The thick red line above the complex terrain are outliers indicating a heavily skewed distribution.

load histories with only a slight increase in the amount of load cycles in the range of about 250 kNm for the complex domain. Not well represented in this figure is the size of the largest load cycles which are close to 3 MNm for the complex domain while they are only half that for the flat domain. In terms of fatigue this is a significant increase. One can however argue that the 600 s time interval over which the response is evaluated is not gathering enough cycles to accurately convey the increase in fatigue since observed cycles are only around 300 as shown in Table 4.2. To capture more cycles the simulated time could be increased.

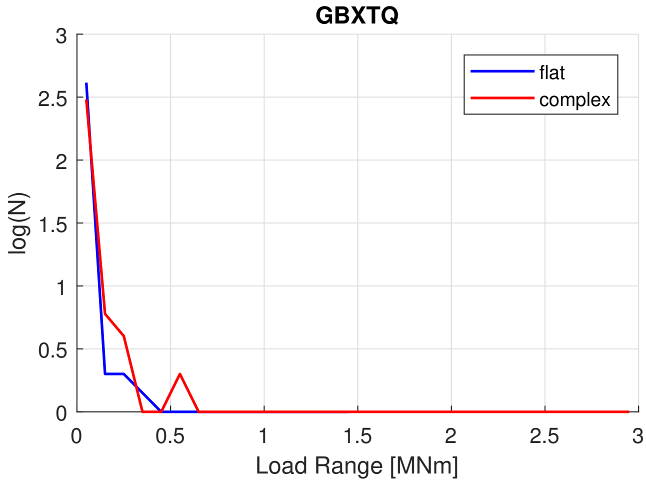

Figure 4.16: Histogram of the load cycles identified over the time history of gearbox shaft torque. The bin width is 100 kNm.

Using the information of the number and size of load cycles from Figure 4.16 the EFL is calculated using equation 2.25. See Table 4.2. As seen the complex domain causes almost double the fatigue on the gearbox shaft as compared to the flat domain even though the total cycle count is similar. This points to the fact that placing a wind turbine on top of a hill/mountain indeed has negative effects on its service life. How much it is reduced is difficult to estimate using these results as the EFL is first and foremost a reference value and does not take into account the multitude of factors which determine actual fatigue. These can be material properties, temperature, multi-axial loads as well as the exact behaviour of the control system installed.

Table 4.2: Equivalent fatigue loads (EFL) of the studied load histories.

	GBXTQ		TBFAM		FWBM		LSSBM	
Domain	EFL	N_c	EFL	N_c	EFL	N_c	EFL	N_c
Flat	0.17	419	3.21	302	2.35	120	0.50	3430
Complex	0.29	319	4.60	274	2.97	114	0.46	4974

Using the same treatment for TBFAM, FWBM and LSSBM as was done for GBXTQ gives the boxplots in Figure 4.17 and the histograms in Figure 4.18 as well as entries of equivalent fatigue loads in Table 4.2. By studying the boxplot of TBFAM in Figure 4.17 it is evident that even though medians lie on similar values, the larger spread of values over complex terrain indicate that TBFAM fluctuates over a larger range in complex terrain than over flat terrain. Also can be seen the numerous outliers caused by the gust. Even if the time history spreads over a larger range the amount of load cycles and their magnitude is very similar as is shown in Figure 4.18. The load range scale of this histogram does not cover the maximum values since these maximums only have individual cycles which are not well represented on a log scale such as this one. The histogram shows that the loads over flat and complex terrain is very similar in nature. Studying the EFL generated by the load histogram of TBFAM in Table 4.2 reveals however that in fact the measured TBFAM over complex terrain is more destructive in terms of fatigue than over flat terrain.

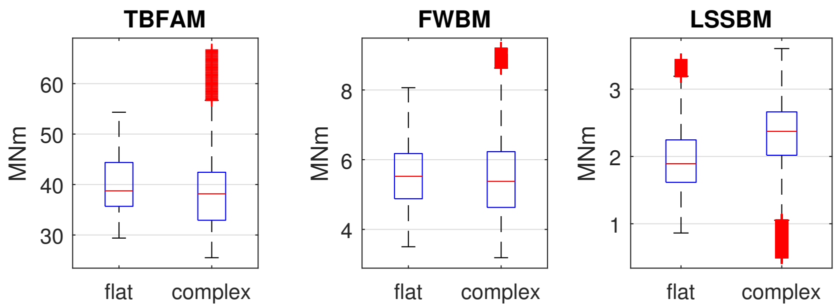

Figure 4.17: Boxplots distributions of tower base-, blade flapwise- and main bearing bending moment.

The distribution of FWBM in the boxplot of Figure 4.17 shows that even in the presence of the gust, the statistical ouliers (marked with red) are fewer than in the case of TBFAM. This seems logical since in the presence of such a gust the blades are pitched to reduce torque on the rotor and effectively reducing strain on the flapwise axis of the turbine blades. The spread is however larger and perhaps this can be related to the slightly positive mean value of the vertical velocity component as was shown in Figure 4.11. The histogram in Figure 4.18 reveals a slight increase in load cycles in ranges above 2 MNm. This results in added fatigue and indeed this is confirmed with a higher EFL for FWBM over complex terrain than over flat terrain as shown in Table 4.2. The captured cycles are only around hundred for both cases of flat and complex terrain but to reach a more representative quantity perhaps a longer simulation time should have been used.

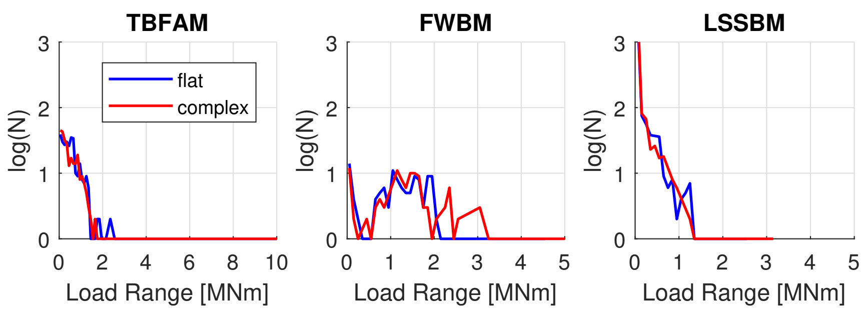

Figure 4.18: Histograms of the identified load cycles of tower base-, blade flapwise- and main bearing bending moment. The bin width is 100 kNm.

Finally the distribution of LSSBM in Figure 4.17 shows that LSSBM behaves somewhat differently than all other variables studied previously. Instead of frequent outliers in the top range of values over complex terrain the situation is now reversed with outliers being present in the top range over flat terrain. There are also numerous outliers found over flat terrain but these are now located below the distribution. Perhaps it is due to the fact that the mean velocity field generated over complex terrain was more constant with altitude than over flat terrain as shown in Figure 4.6. This means that the difference in mean wind velocity at lower and higher altitudes for flat terrain are effectively causing an increased LSSBM as compared to complex terrain where the velocity was more equal over the rotor disk. The overall higher distribution over the complex terrain is perhaps caused rather by increased lateral fluctuations. By inspecting the individual load cycles shown in Figure 4.18 shows that the load histories over flat and complex terrain are very similar. There are some slightly higher load cycles that are identified over flat terrain. The EFL in Table 4.2 confirms that in terms of fatigue the load histories are very similar although here the flat terrain seems to be more destructive even though the identified load cycles are fewer.

5

Conclusion

In this study, applying the numerical models, generating a domain of Rödbergskullen and attaining the results for use with the aero-elastic solver went well. The RANS wind field generated is a valuable tool to use as reference for DES/LES simulations. The transient wind field generated by DES proves to be too protective of the boundary layer. The result is that it dampens most fluctuations in the vicinity of the ground making it unsuitable for determining the dynamic response of a wind turbine.

LES obtains velocity profiles that are very close too that which is predicted by RANS even without the use of any rough wall treatment. Perhaps this is because the relatively large length scales found in ABL flow making it possible to model the outer flow with a good resolution. In LES the resolved turbulent kinetic energy in the vicinity of the wind turbine is also close to what is predicted by RANS. Despite a fairly good representation of turbulent quantities in the lower altitudes of the LES it can not be overlooked that the symmetric boundaries imposed on the top of the domain causes an unrealistic drop in Reynolds stresses at altitudes above 700 m. It is therefore recommended that symmetric boundaries be avoided for any future LES studies of an ABL. The Reynolds stresses and other time-averaged components of the study also show evidence that the sampling time used is too short. The sampling time used is roughly the time of one flow pass so for future studies a longer sampling time is preferable. Given the relatively coarse near wall mesh resolution used in this study a thorough mesh independence study is recommended.

By studying the wind components as functions of time it is evident that they are lacking in any higher frequencies. Although it is debatable whether these higher frequencies affect the wind turbine response in any great manner it may be interesting to further decrease the cell size. Both to investigate if any higher frequencies can be captured and whether the effect of these higher frequencies is significant on the operation of the wind turbine. However LES is computationally costly and so all efforts should be made to decrease these costs. One way might be to decrease the size of the domain as this will decrease the cell count dramatically. Perhaps it is most feasible to cut away sections in the downwind fetch of the area of interest but the effect of this should then be studied.

If the discrepancies of the Reynolds stresses should be overlooked the difference of the flow over flat and complex terrain is found to be such that the time-averaged velocity over complex terrain is higher than over flat terrain. This is expected as wind speed-up over hills/mountains is a well documented phenomena. However by looking at the wind velocity as a function of time the behaviour is such that in both cases wind fluctuates around a similar value most of the time. It is only what can be described as a gust that increases the time-averaged velocity over complex terrain resulting in the time-averaged speed-up. With a simulation time of 10 minutes it is however recommended that a longer simulation time be used before a conclusion of this sort be made. The response of the turbine shows that the placement of a wind turbine in complex terrain causes an increased amount of fatigue. This is even though the turbulent intensity decreases over complex terrain. The cause of this is likely to be the gust of wind that appears over the complex terrain. The simulation time of 10 minutes does however limit the amount of periodic phenomena such as gusts as well as the amount of total load cycles captured. To reach a better statistical representation the simulations time should therefore be increased in any future studies.

Due to the discrepancies found in both simulation time and measured turbulence near boundaries this study did perhaps not reach its original goal of quantifying the effects of complex terrain. It did however demonstrate the potential of LES and will hopefully prove useful in further studies of similar nature.

Bibliography

[1] ASTM. (1985) Standard practices for cycle counting in fatigue analysis. Technical Report, ASTM-E1049-85, American Society for Testing and Materials, West Conshohocken, PA.

[2] Bechmann, A. (2006) Large-Eddy Simulation of Atmospheric Flow over Complex Terrain. Roskilde: Risø National Laboratory, Risø-PhD-28(EN).

[3] Bechmann, A., Sørensen, N.N. (2011) Hybrid RANS/LES applied to complex terrain. DOI: 10.1002/we. Wind Energy (14:225-237).

[4] Blocken, B., van der Haut, A., Dekker, J., Weiler, O. (2015) CFD Simulation of Wind Flow Over Natural Complex Terrain: Case Study with Validation by Field Measurements for Ria de Derrol, Galicia, Spain. Journal of Wind Engineering and Industrial Aerodynamics, 147 (2015) 43-57.

[5] Davidson, L. (2017) An Introduction to Turbulence Models. Chalmers University of Technology, Goteborg, Sweden.

[6] Davidson, L. (2018) Fluid mechanics, turbulent flow and turbulence modeling. Chalmers University of Technology, Goteborg, Sweden.

[7] Energimyndigheten: Vindkraftens del av elförsörjningen, `http://www.energimyndigheten.se/fornybart/vindkraft/`

[8] Hendriks, H.B., Bulder, B.H (1995) Fatigue Equivalent Load Cycle Method: A General Method to Compare Fatigue Load of Different Load Spectrums. Energy Research Centre of the Netherlands (ECN), ECN-C–95-074

[9] Ingram, G. (2018) Wind Turbine Blade Analysis using the Blade Element Momentum Method. Durham University, Durham, England.

[10] Jonkman, J., Butterfield, S., Musial, W., Scott, G. (2009) Definition of a 5-MW Reference Wind Turbine for Offshore System Development. National Renewable Energy Laboratory, 1617 Cole Boulevard, Golden, Colorado

[11] Kim, H.G, Patel, V.C, Lee, C.M. (2000) Numerical Simulation of Wind Flow Over Hilly Terrain. Journal of Wind Engineering and Industrial Aerodynamics, 87 (2000) 45-60.

[12] Menter, F.R., Kuntz, M. (2002) Adaptation of Eddy Viscosity Turbulence Models to Unsteady Separated Flows Behind Vehicles, The Aerodynamics of Heavy Vehicles: Trucks, Buses and Trains. Springer, Asilomar, CA.

[13] Nebenführ, B., Davidson, L. (2017) Prediction of wind-turbine fatigue loads in forest regions based on turbulent LES inflow fields. DOI: 10.1002/we. Wind Energy (20:1003–1015).

[14] Richards, P.J., Hoxey, R.P. (1993) Appropriate boundary conditions for computational wind engineering models using the k-ε turbulence model. J. Wind Eng. Ind. Aerodyn. 46–47, 145–153.

[15] Taylor, P.A., Teunissen, H.W. (1983) Askervein '82: Report on the September/October 1982 Experiment to Study Boundary Layer Flow Over Askerveint, South Uist. Atmospheric Environment Service, Downsview, Ontario (Report MSRB-83-8).

[16] Taylor, P.A., Teunissen, H.W. (1985) The Askervein Hill Project: Report on the September/October 1983 Main Field Experiment. Atmospheric Environment Service, Downsview, Ontario (Report MSRB-84-86).

[17] Taylor, P.A., Teunissen, H.W. (1987) The Askervein Hill Project: overview and background data. Boundary-Layer Meteorological. 39 (1-2), 15-39.

[18] OX2, Sweden,
`http://www.ox2.com/projekt/robergsfjallet/`

[19] Troen, I., Lundtang Petersen, E. (1989). European Wind Atlas. Roskilde: Risø National Laboratory.

[20] Gerasimov, A. (2016) Quick Guide to Setting Up LES-type Simulations, version 1.4. European Technology Group, Ansys, Sweden.

[21] Zikanov, O. (2010) Essential computational fluid dynamics. John Wiley & Sons, Inc., Hoboken, New Jersey.

A

Wind measurements over Rödbergskullen

Prior to this study, wind data has been accumulated at a meteorological mast located on Rödbergskullen. The mast provides measurements at an hourly rate, spanning the full year of 2016. The measurements are comprised of an average and standard deviation of wind speed and direction at a height of 60 m a.g.l. This data is analysed for dominating wind speeds, turbulent intensity and wind direction for choosing relevant inlet boundary conditions. In summary: wind speeds are most common in the range of 6-8 m/s with a turbulent intensity of about 13%. Dominant wind direction is 225° with respect to the north.

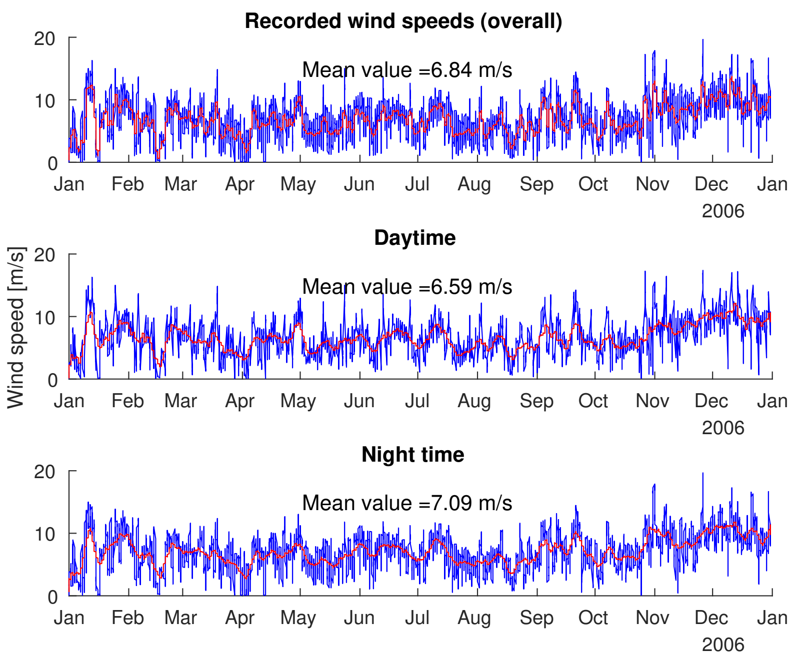

Figure A.1: Wind speed average measurements over Rödbergskullen. This figure compares the overall measurements to those measured only by daytime or night time. Day was assumed as the hours between 6:00-18:00. Blue lines represent measured values while the red lines represent a moving 72 hour average.

Figure A.1 shows the hourly wind speed average as it was measured over Rödbergskullen throughout the year 2016. Topmost are the overall measurements but below are the same results filtered as to show only daytime and nighttime measurements. The average values at day and night time are relatively close to 7 m/s indicating there is no great change in wind speed between day and night. A histogram of the the average velocities is shown in Figure A.2. It further underlines that the most common wind speeds are between 6-8 m/s. In fact the wind speed is in the range of 5-8 m/s more than 40% of the time.

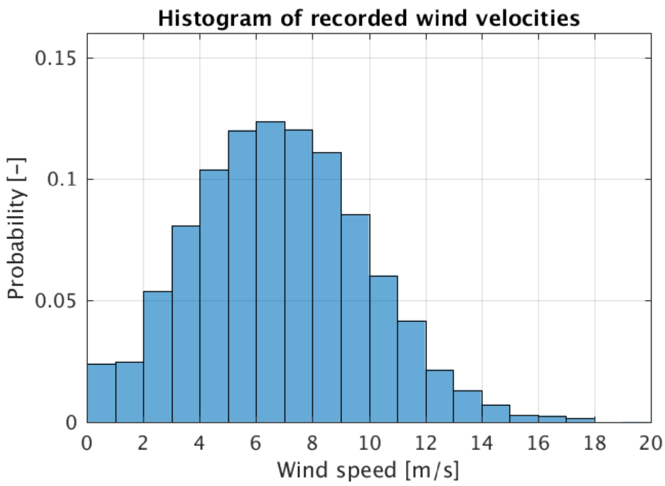

Figure A.2: Histogram of recorded wind speed averages. This representation includes both day and night time measurements.

The measured wind direction is shown in Figure A.3. With a bin size of 30 degrees it shows that the prevailing wind directions over Rödbergskullen are southwesterly winds from a heading of roughly 225°. There is not a great difference when looking only at wind speeds between 6-8 m/s or the total dataset.

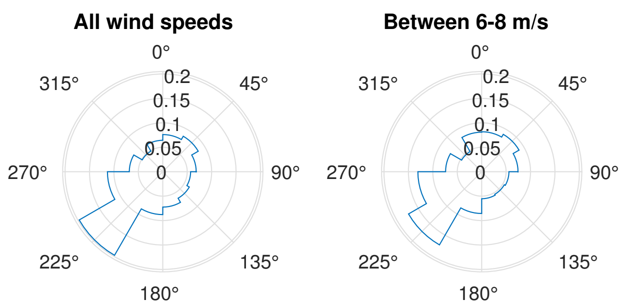

Figure A.3: Histogram of recorded wind direction averages. This representation includes both day and night time measurements.

Averages of measured turbulent intensity are shown as a function of mean wind speed in Figure A.4. Also marked in the figure is the reach of standard deviation. For lower wind speeds the turbulent intensity is larger with larger variance but above 6 m/s the turbulent intensity is almost constant at value of about 13% with a standard deviation of 3%.

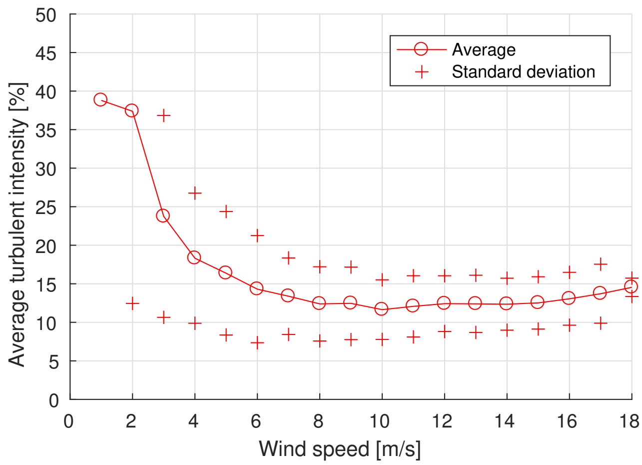

Figure A.4: Recorded turbulent intensity. This representation includes both day and night time measurements.

The topography of Rödbergskullen and the surrounding area is shown in Figure A.5. Rödbergskullen itself is located on the centre and contrasts well as it is the highest point on the topography map (red area in centre image). The lowest and highest elevations in the area range from 250 m to 540 m. Not seen in the topography are any structures on the ground surface which is partly covered with farmlands and partly by dense patches of forest.

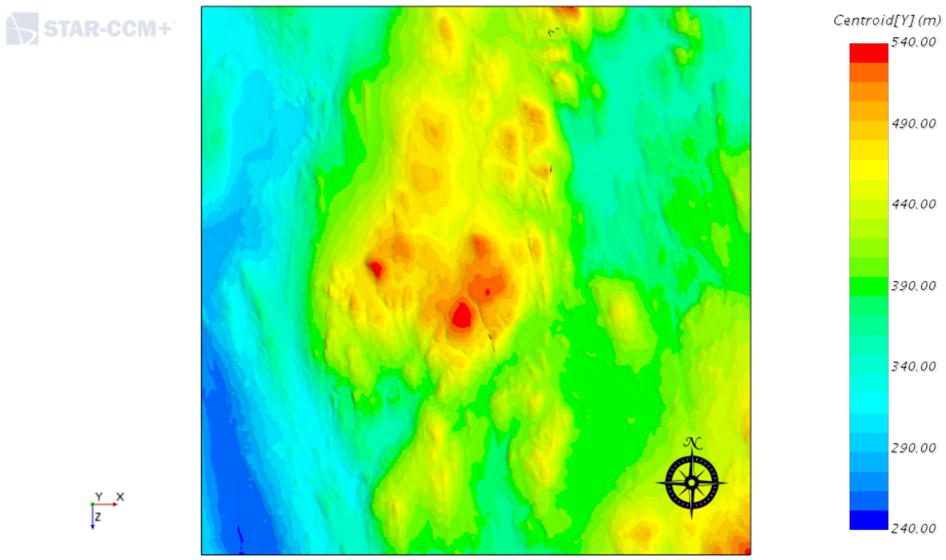

Figure A.5: Map of the area in study. Rödbergskullen is the red area in the centre of the image with a maximum elevation of 540m.